XXV European Cosmic Ray Symposium
4-9 September 2016

Measurement of the properties of cosmic rays with the LOFAR radio telescope

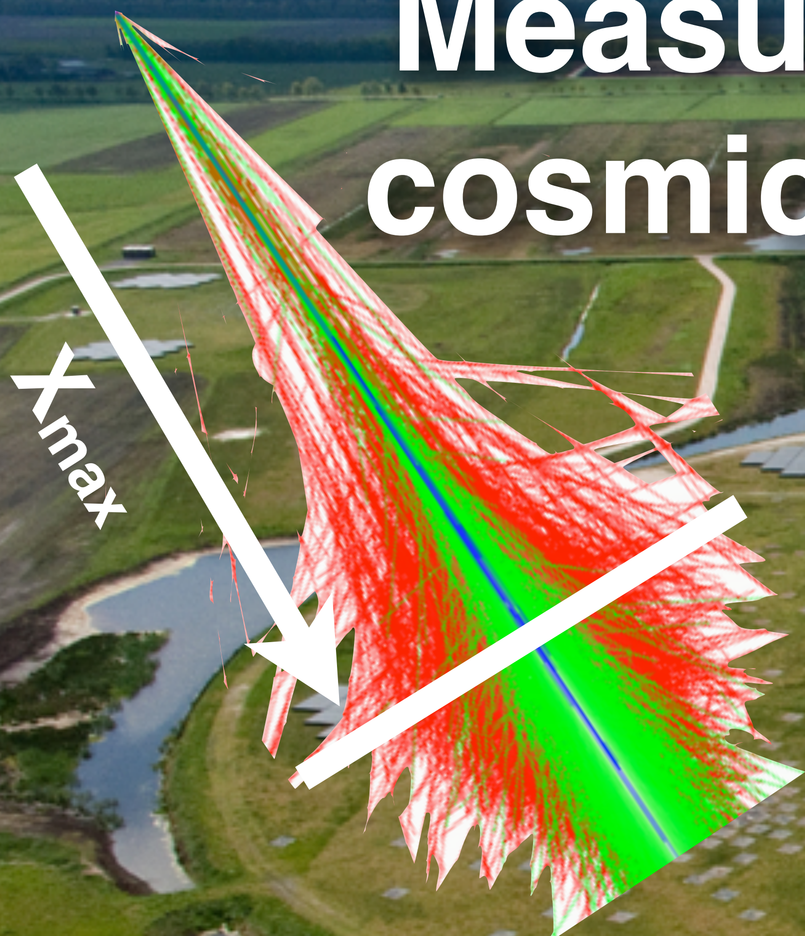

characterize cosmic rays:
- -direction
- -energy
- -mass

@100% duty cycle

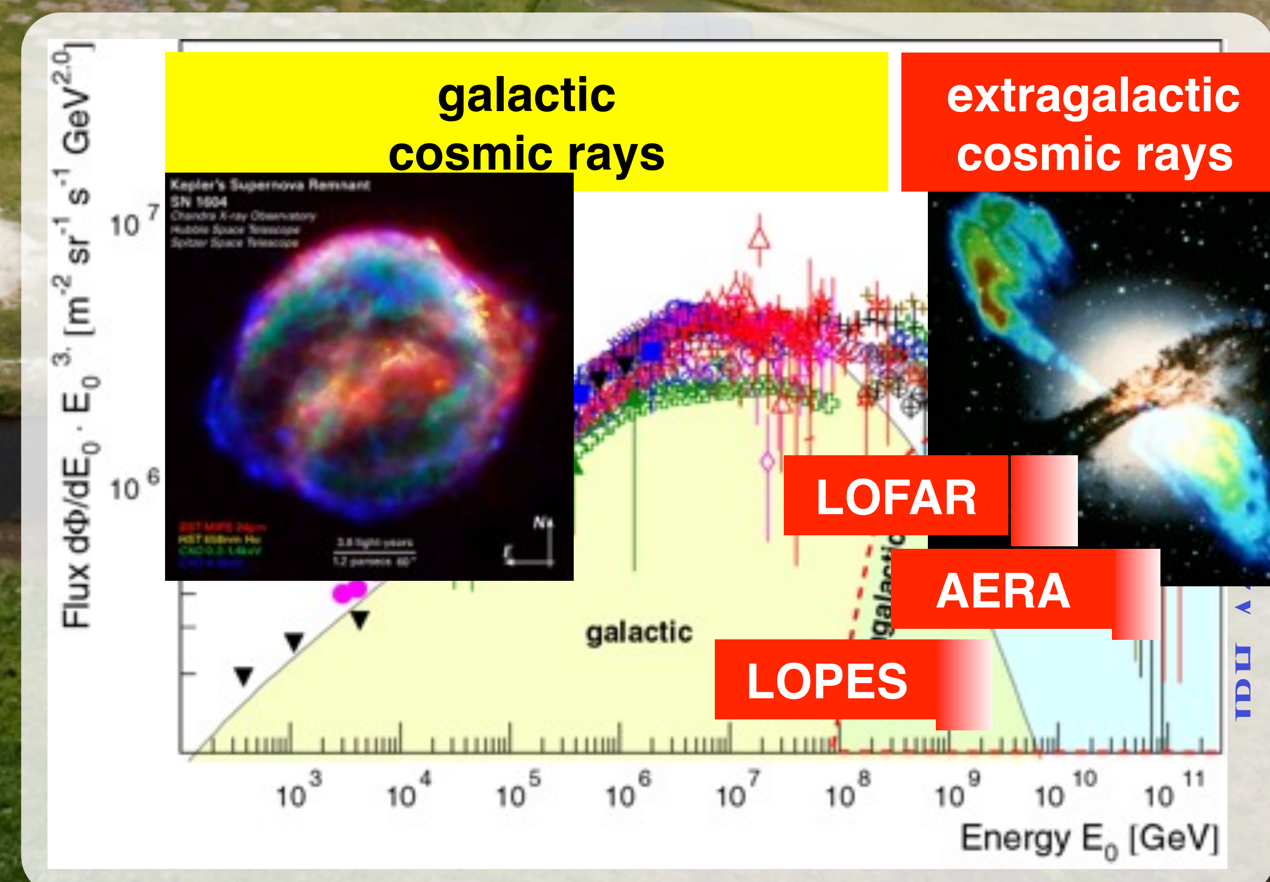

Jörg R. Hörandel Radboud University Nijmegen & Nikhef http://particle.astro.ru.nl

LOFAR

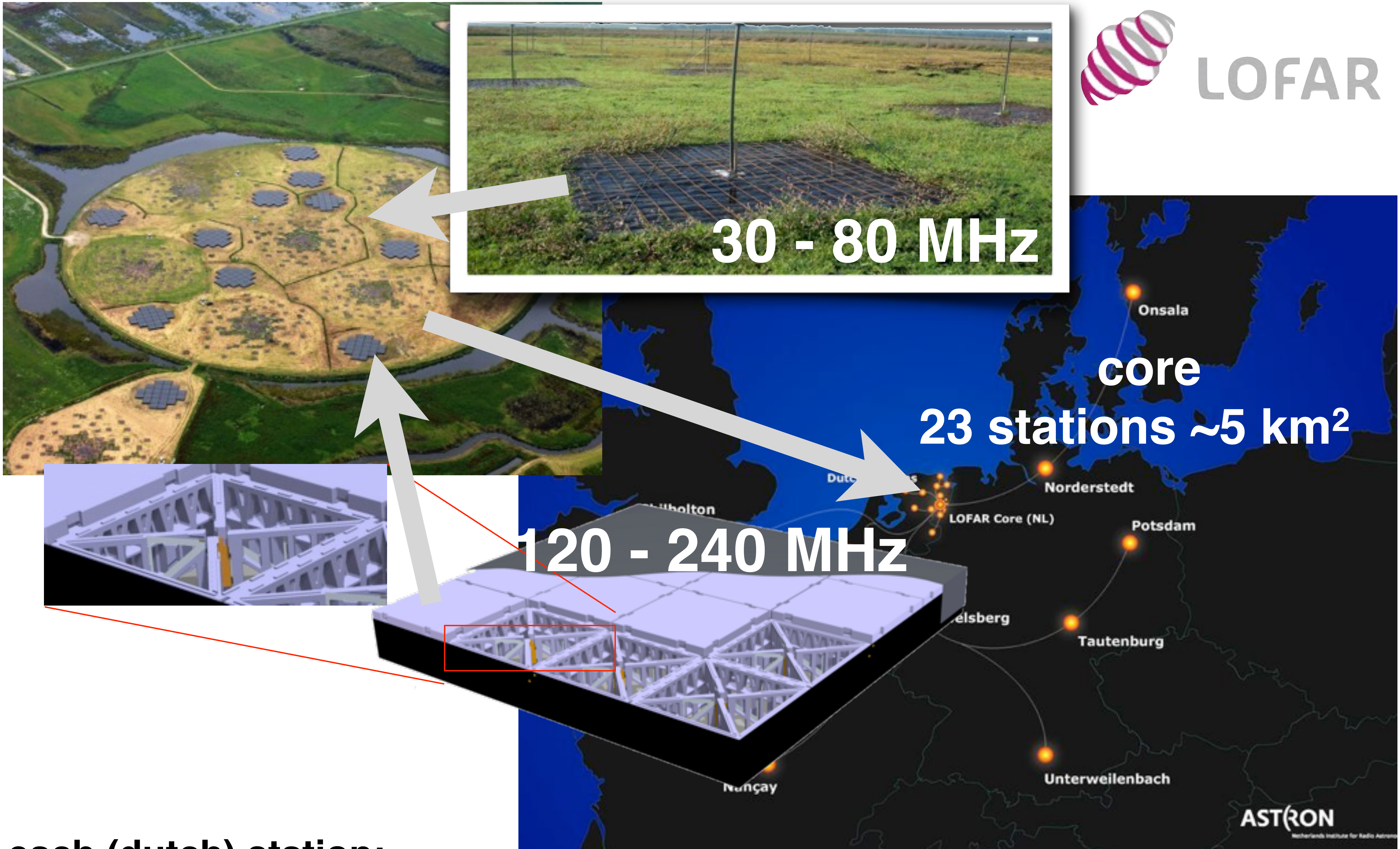

each (dutch) station:
- 96 low-band antennas 30- 80 MHz
- high-band antennas (2x24 tiles) 120-240 MHz

M. van Haarlem et al., A&A 556 (2013) A2

LOFAR Radboud Air Shower Array - LORA

20 scintillator units (~1 m² each) in LOFAR core

➡ **provide**

- **properties of EAS**
- **and trigger**

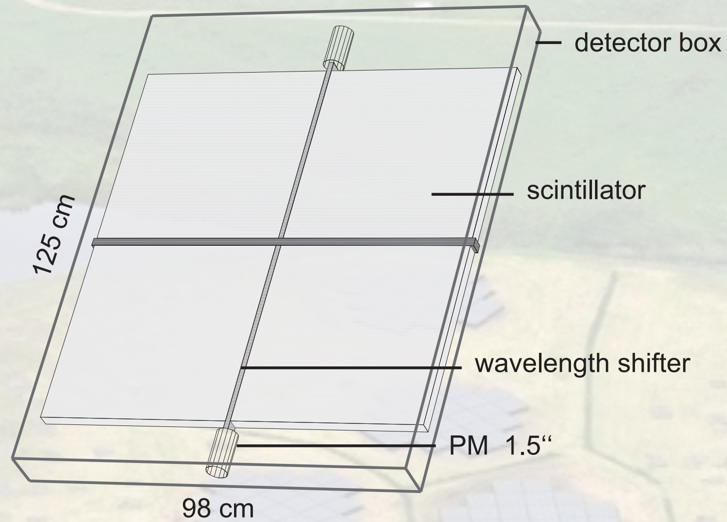

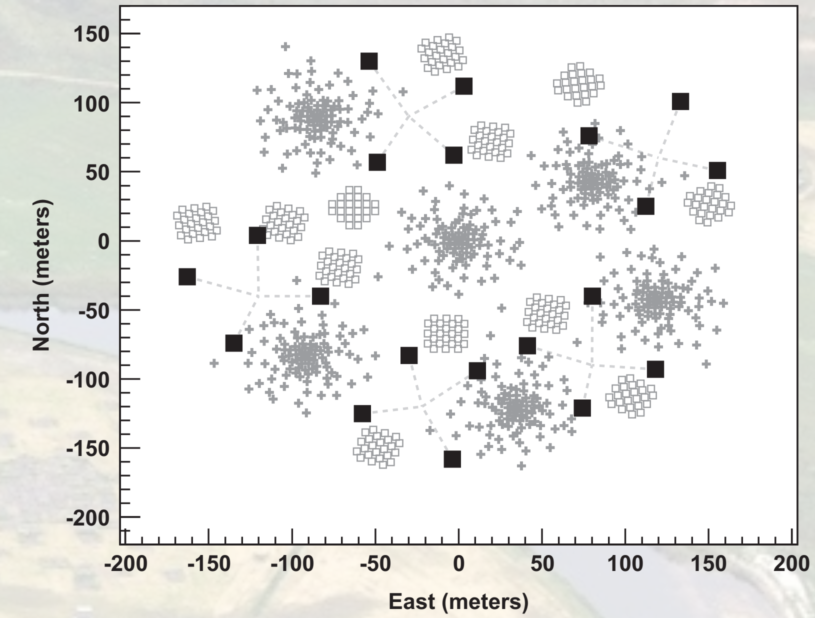

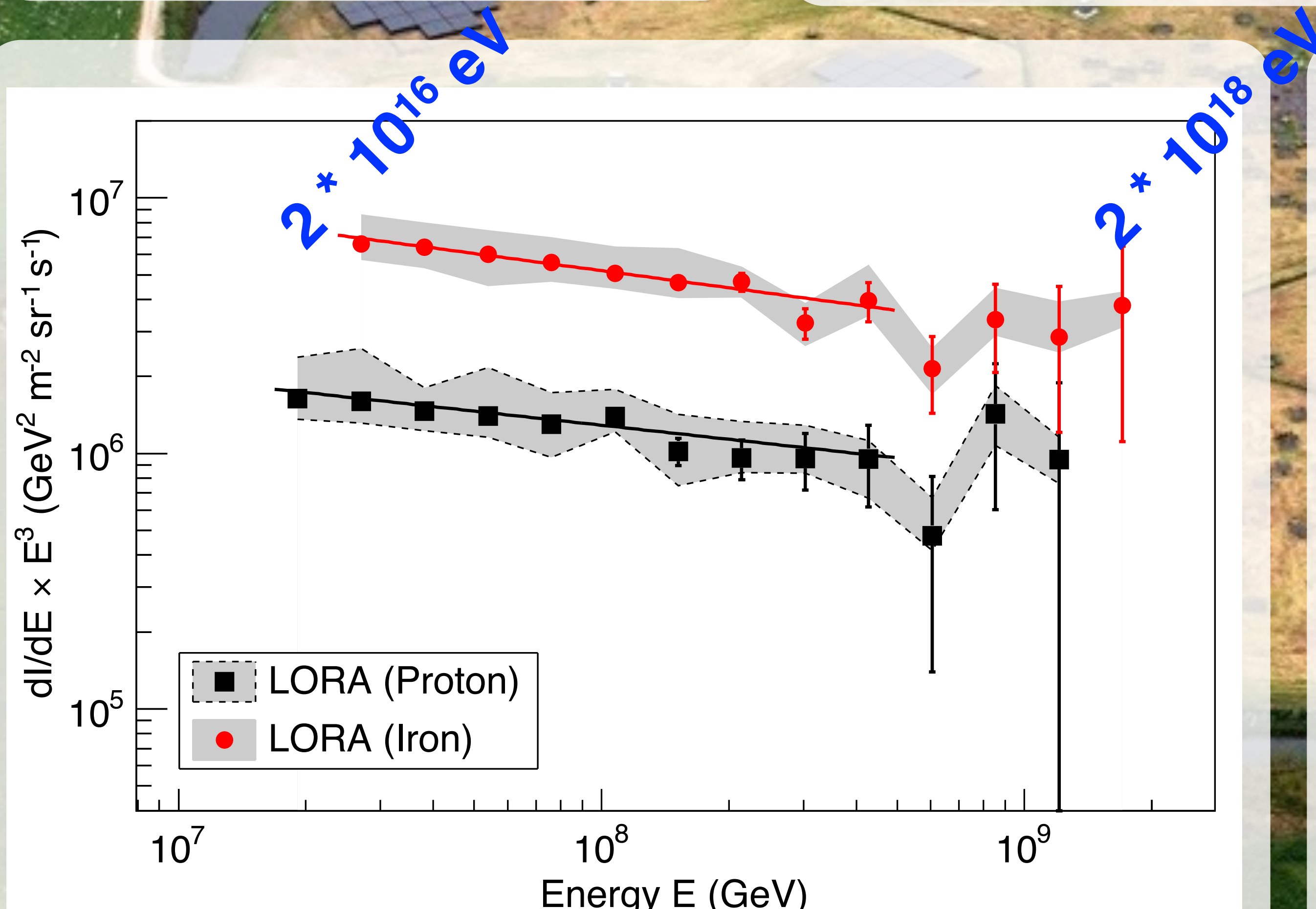

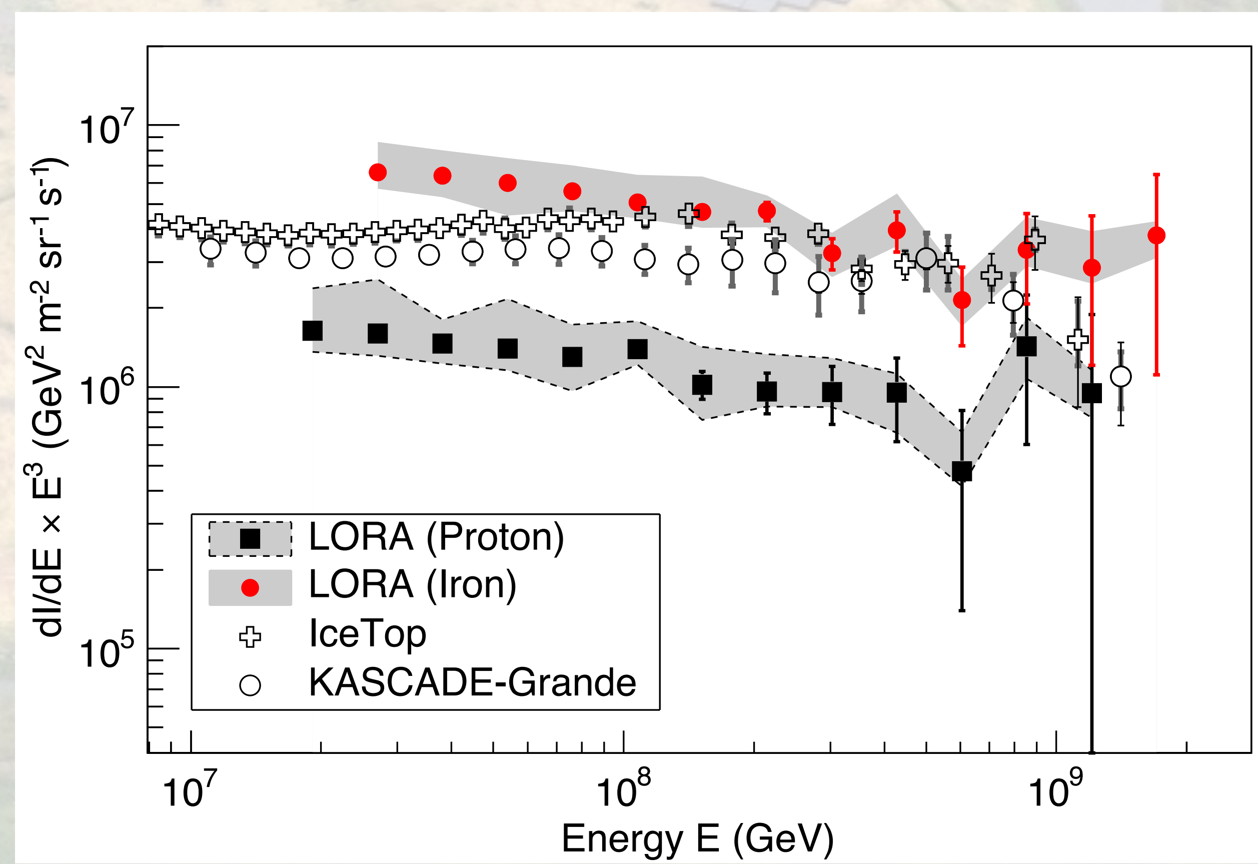

S. Thoudam et al, Nucl. Instr. Meth. A 767 (2014) 339

S. Thoudam et al, Astropart. Phys. 73 (2016) 34

Gain of complete signal chain

with a crane

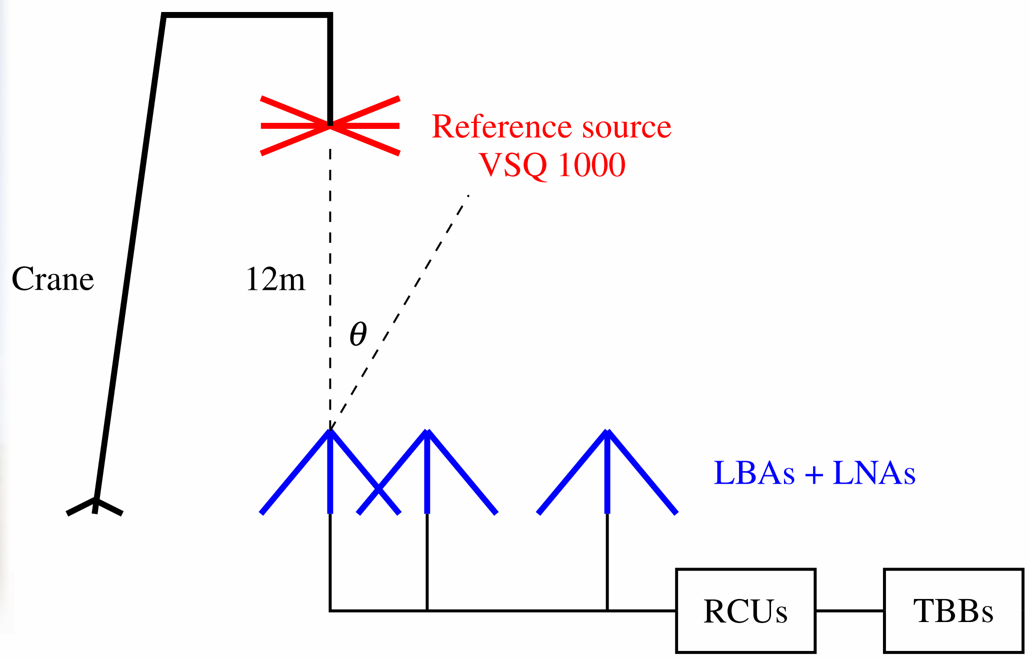

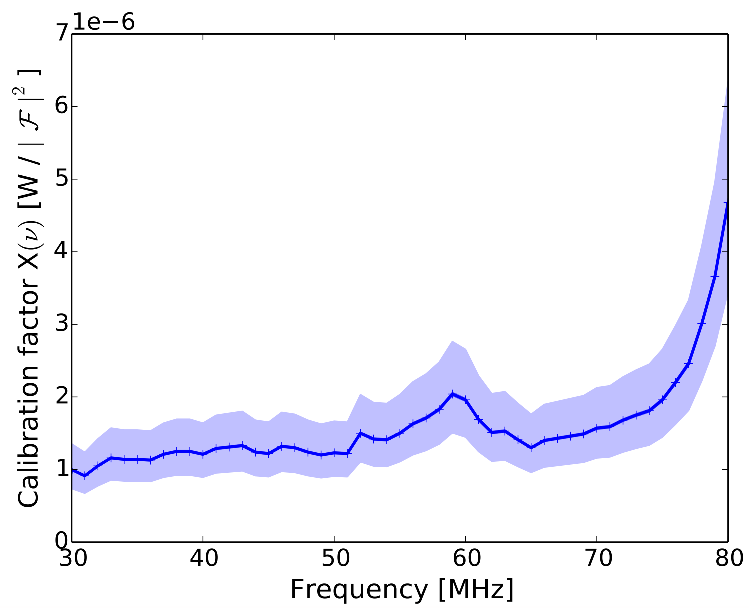

A. Nelles et al, JINST 009 (2015) 0815

Gain of complete signal chain

with a crane

with Galactic emission

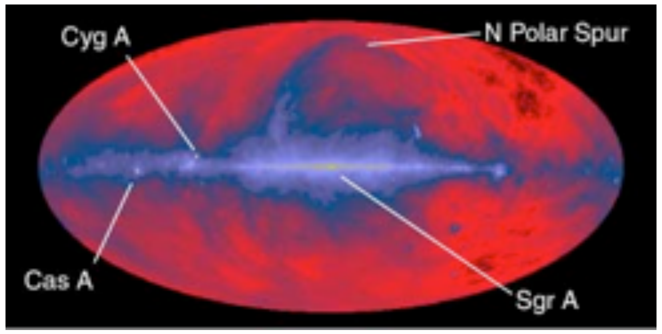

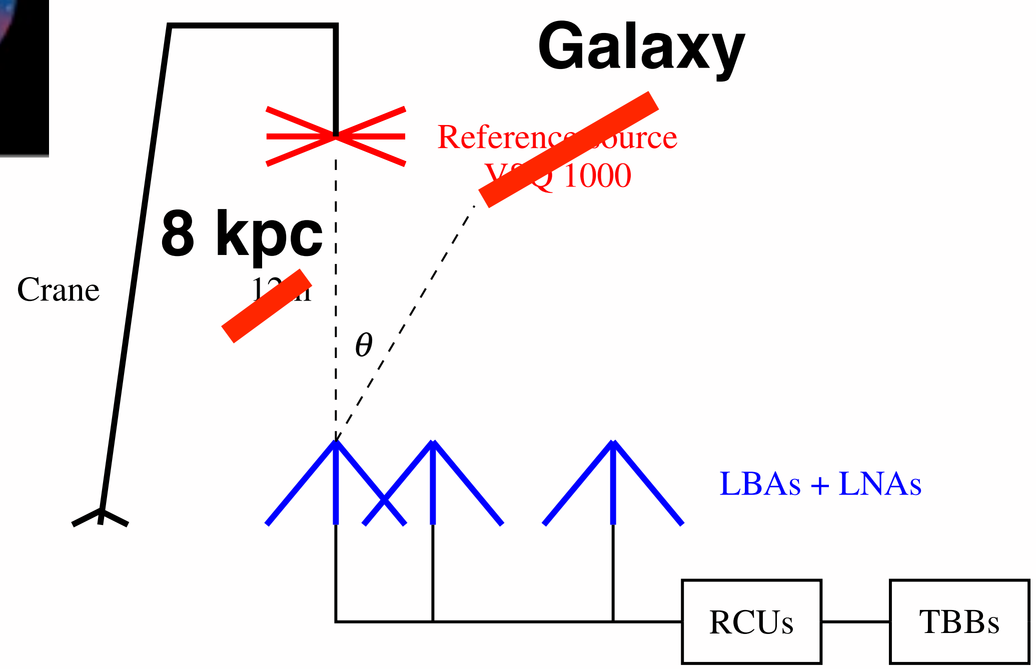

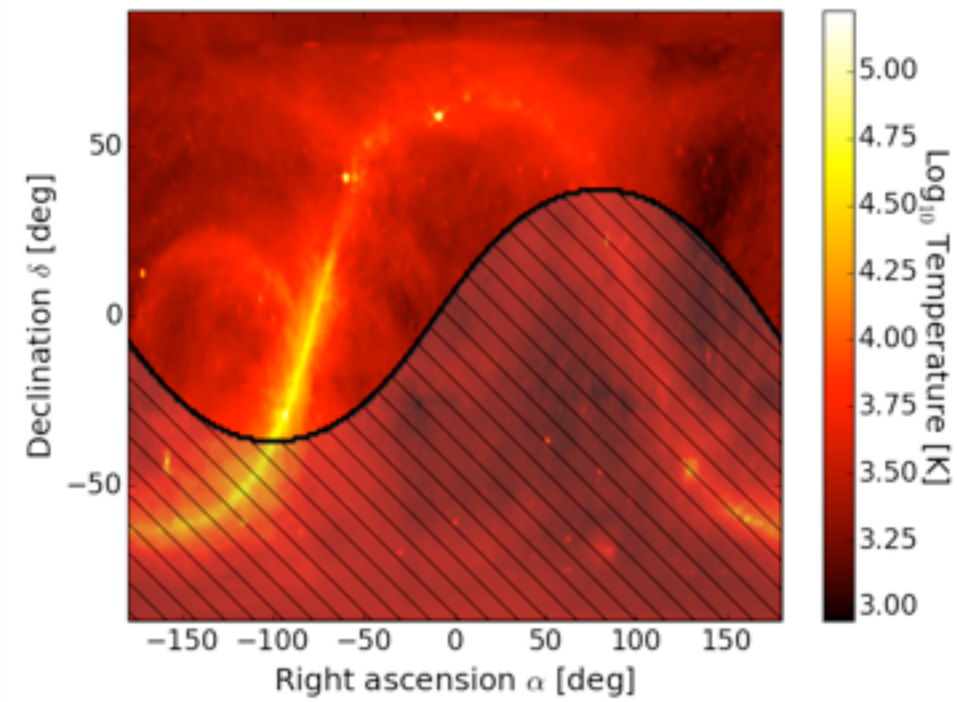

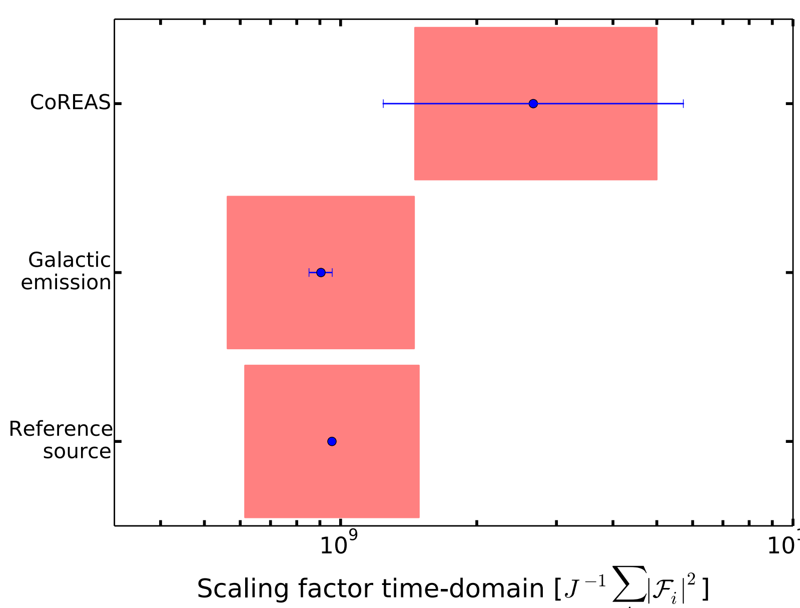

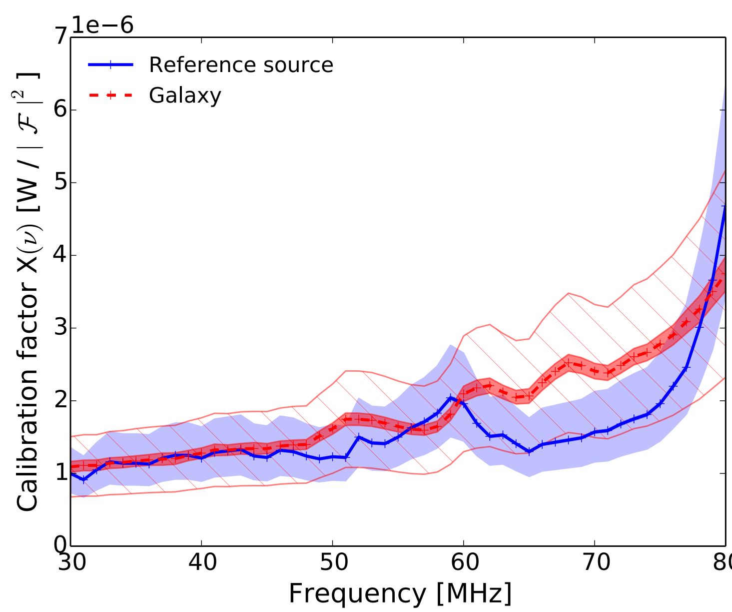

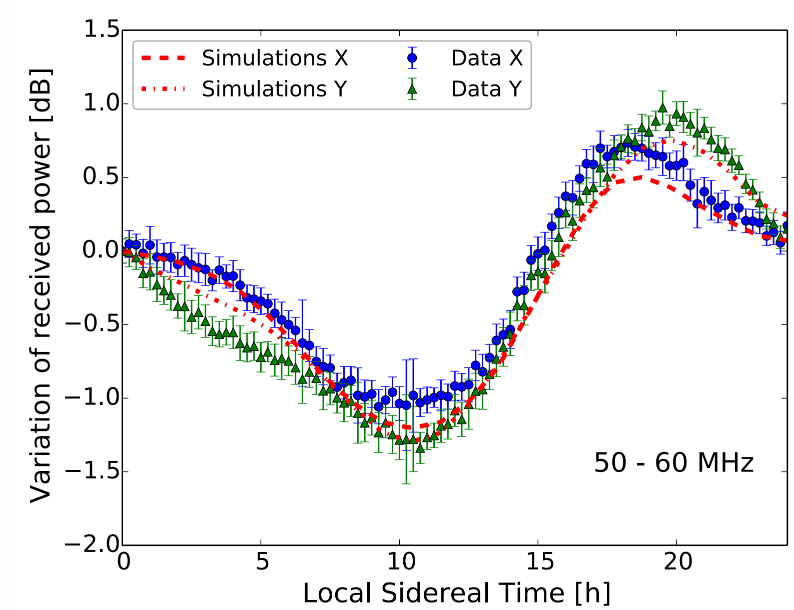

A. Nelles et al, JINST 009 (2015) 0815

A measured air shower

angular difference particles - radio

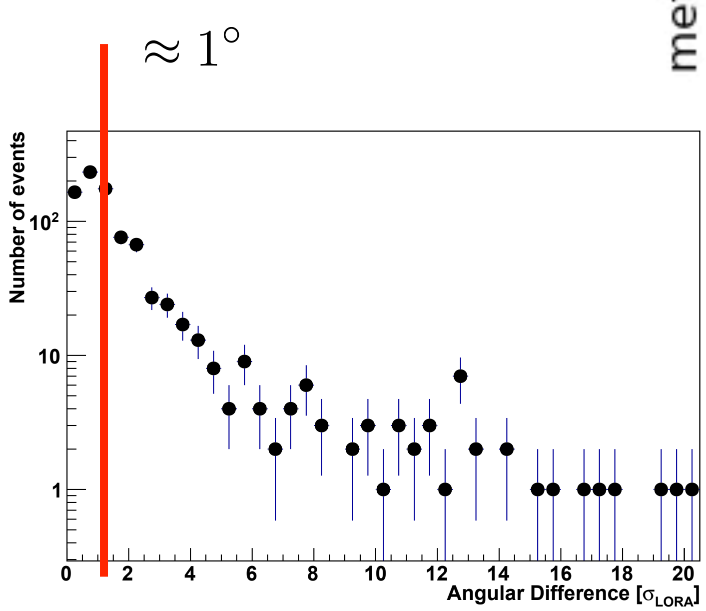

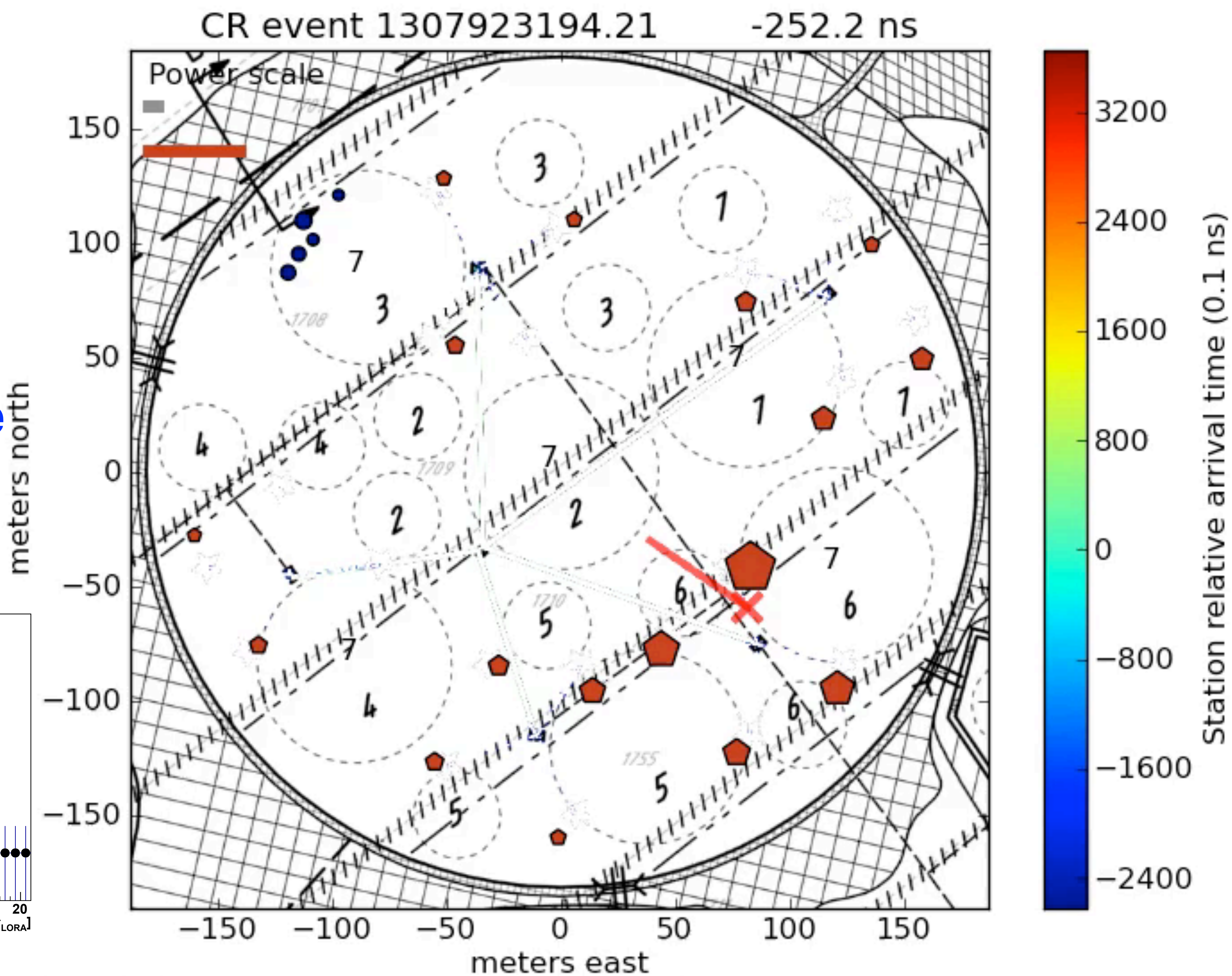

Circles: LOFAR antennas, Pentagons: LORA particle detectors, size denotes signal strength

LOFAR

Radio Emission in Air Showers

- **Mainly: Charge separation in geomagnetic field**

$$\vec{E} \propto \vec{v} \times \vec{B}$$

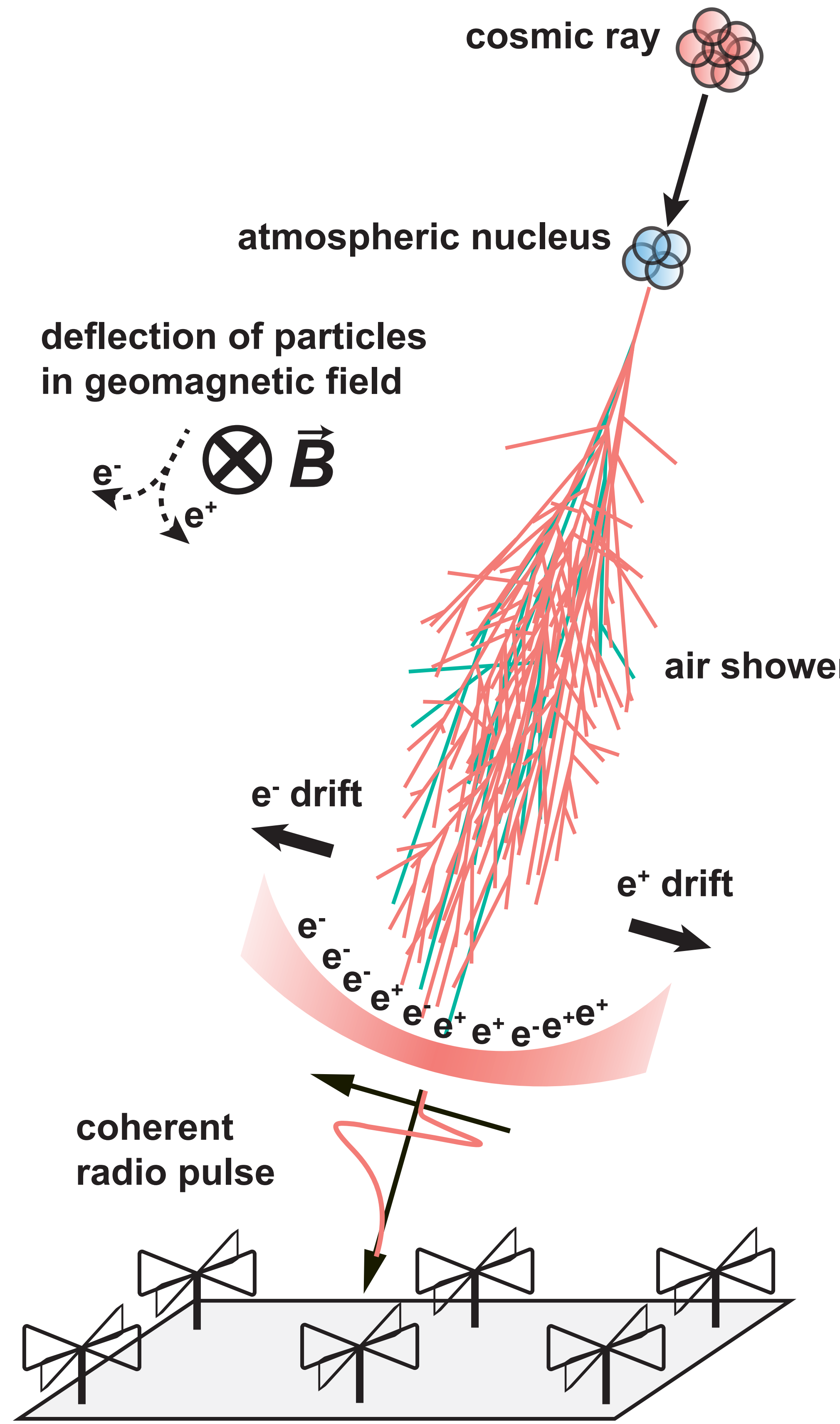

Arrival direction of showers with strong radio signals

north-south asymmetry
v x B effect

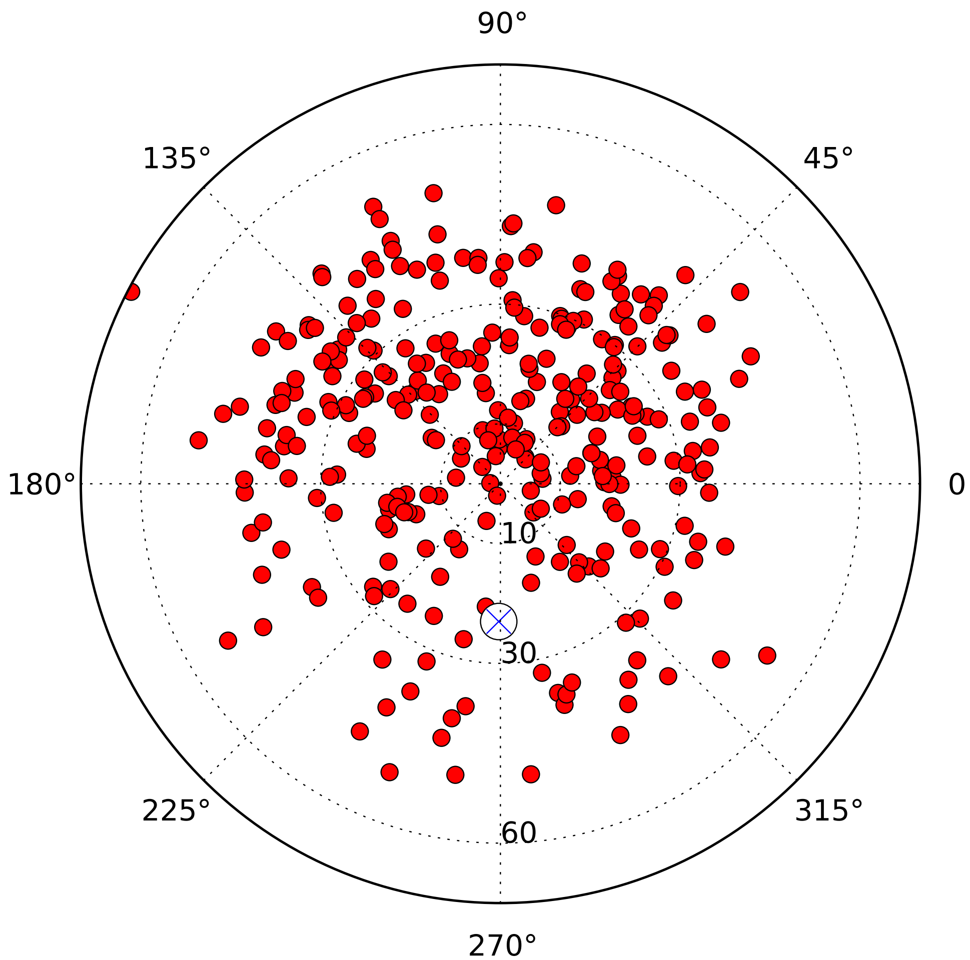

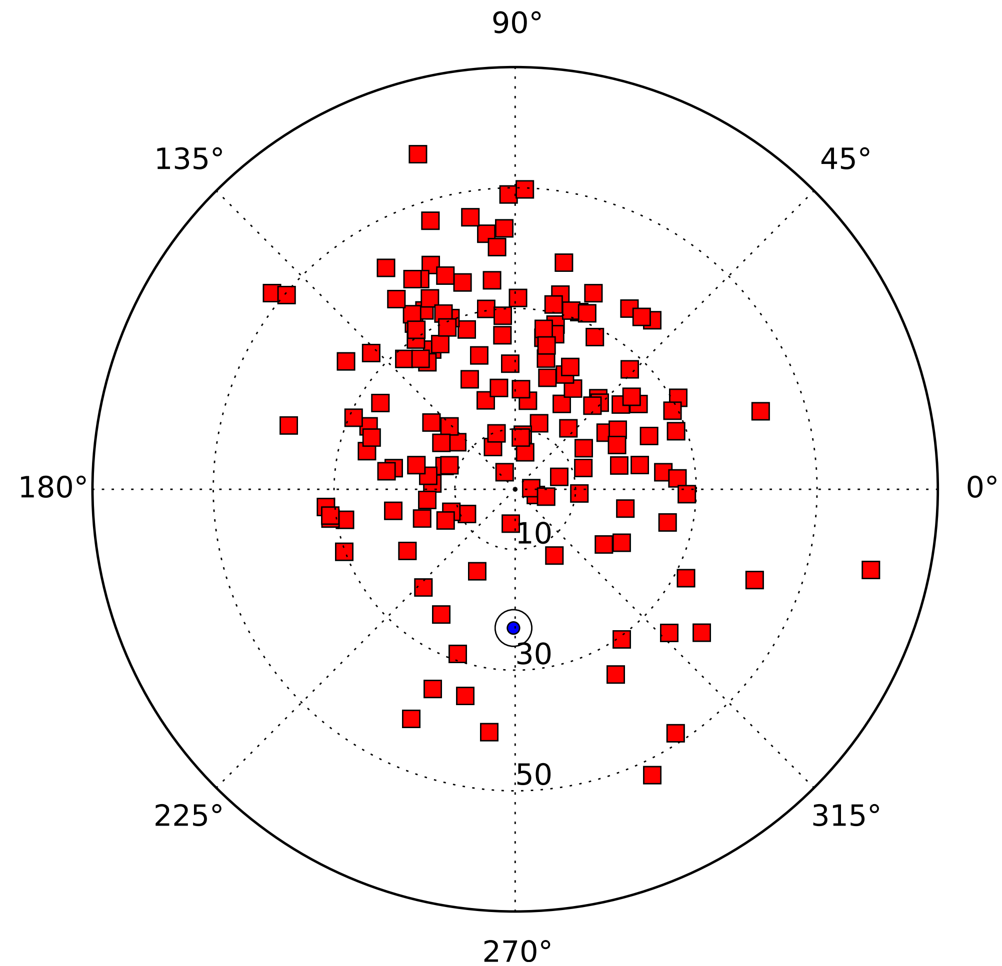

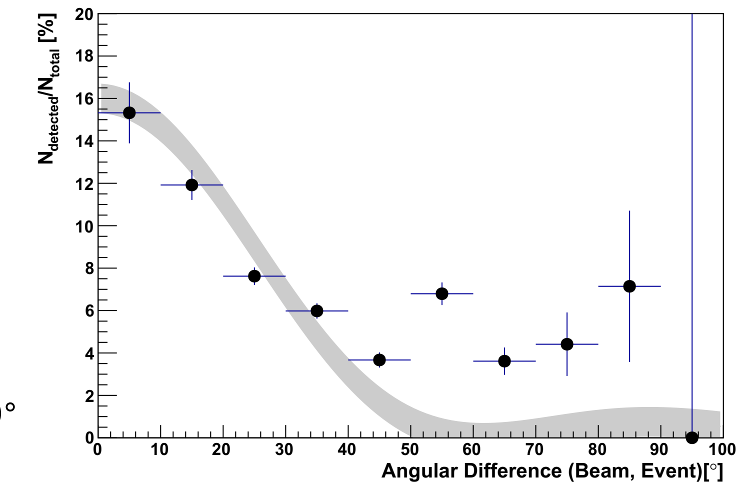

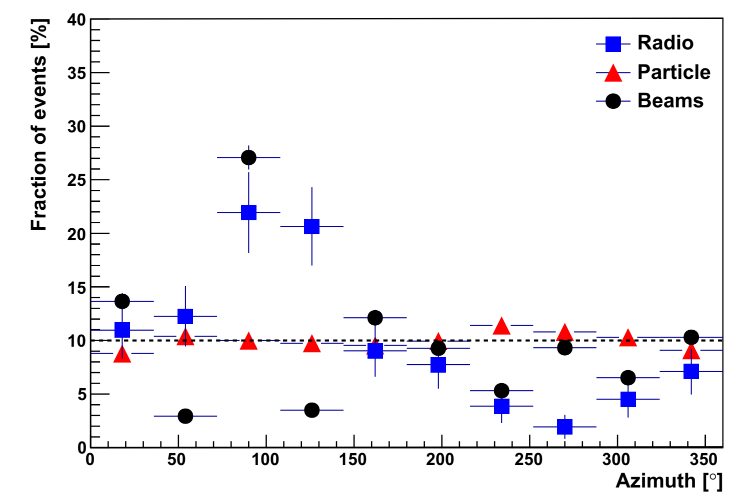

30 - 80 MHz

110 - 190 MHz

P. Schellart et al., A&A 560 (2013) A98

A. Nelles et al., Astroparticle Physics 65

Radio Emission in Air Showers

- Mainly: Charge separation in geomagnetic field

  $\vec{E} \propto \vec{v} \times \vec{B}$

  Theory predicts additional mechanisms:
- excess of electrons in shower: charge excess
- superposition of emission due to Cherenkov effects in atmosphere

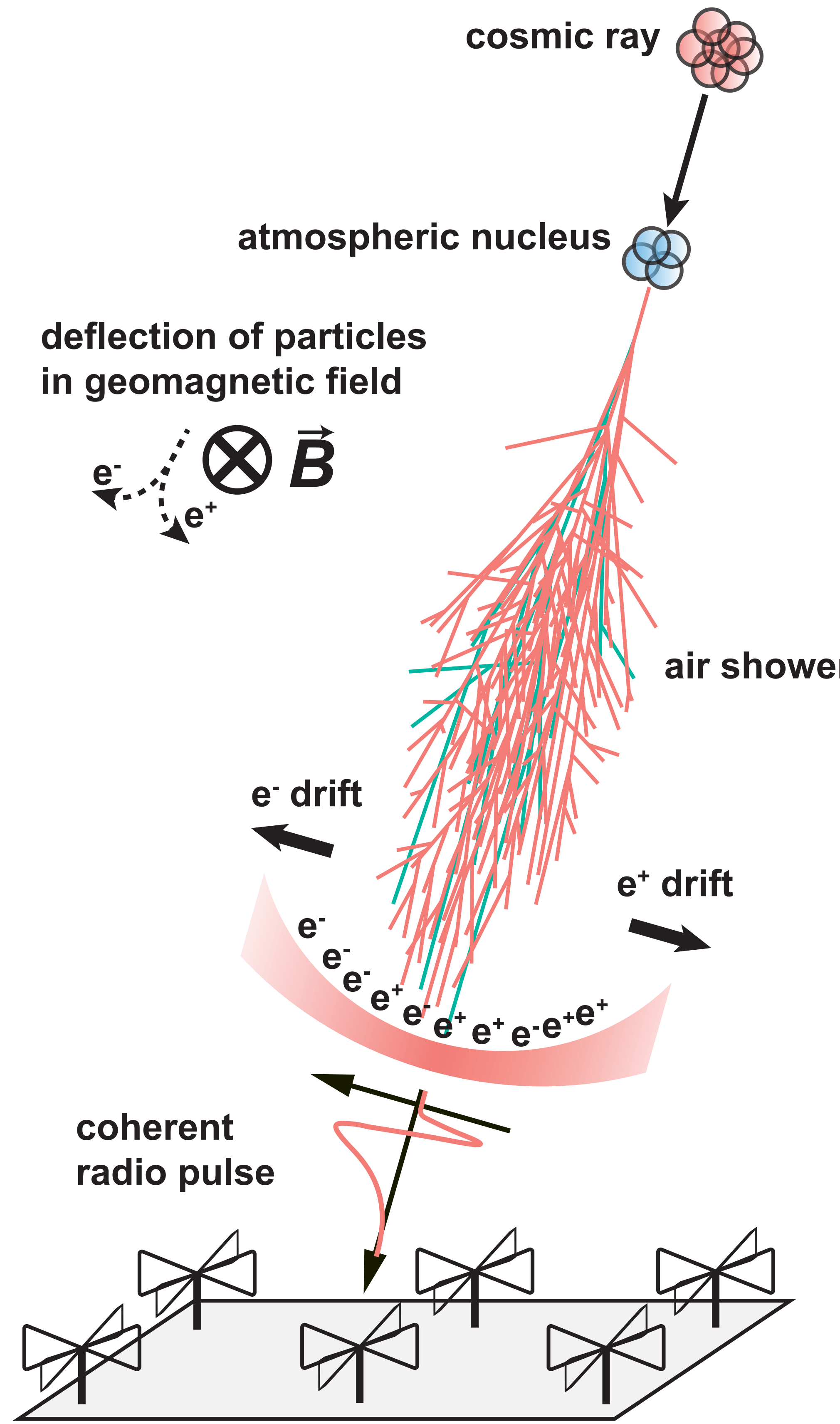

polarization of radio signal

geomagnetic

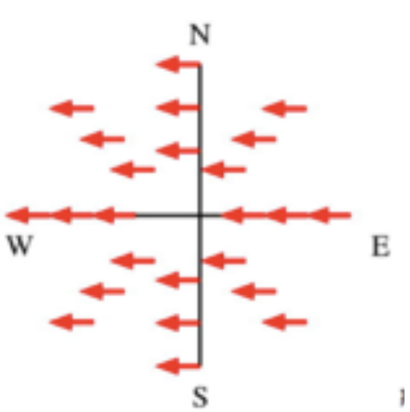

Askaryan

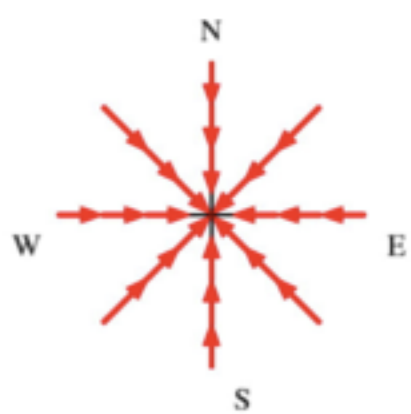

Polarization footprint

of an individual air shower

geomagnetic

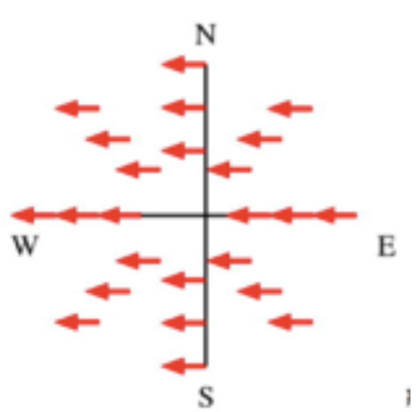

Askaryan

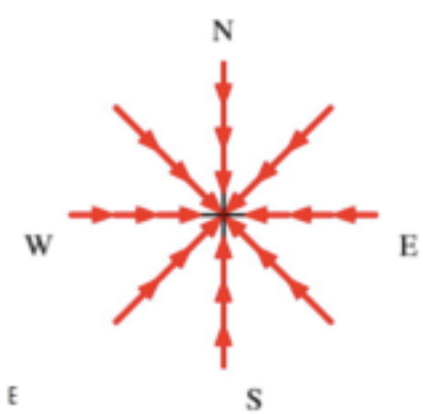

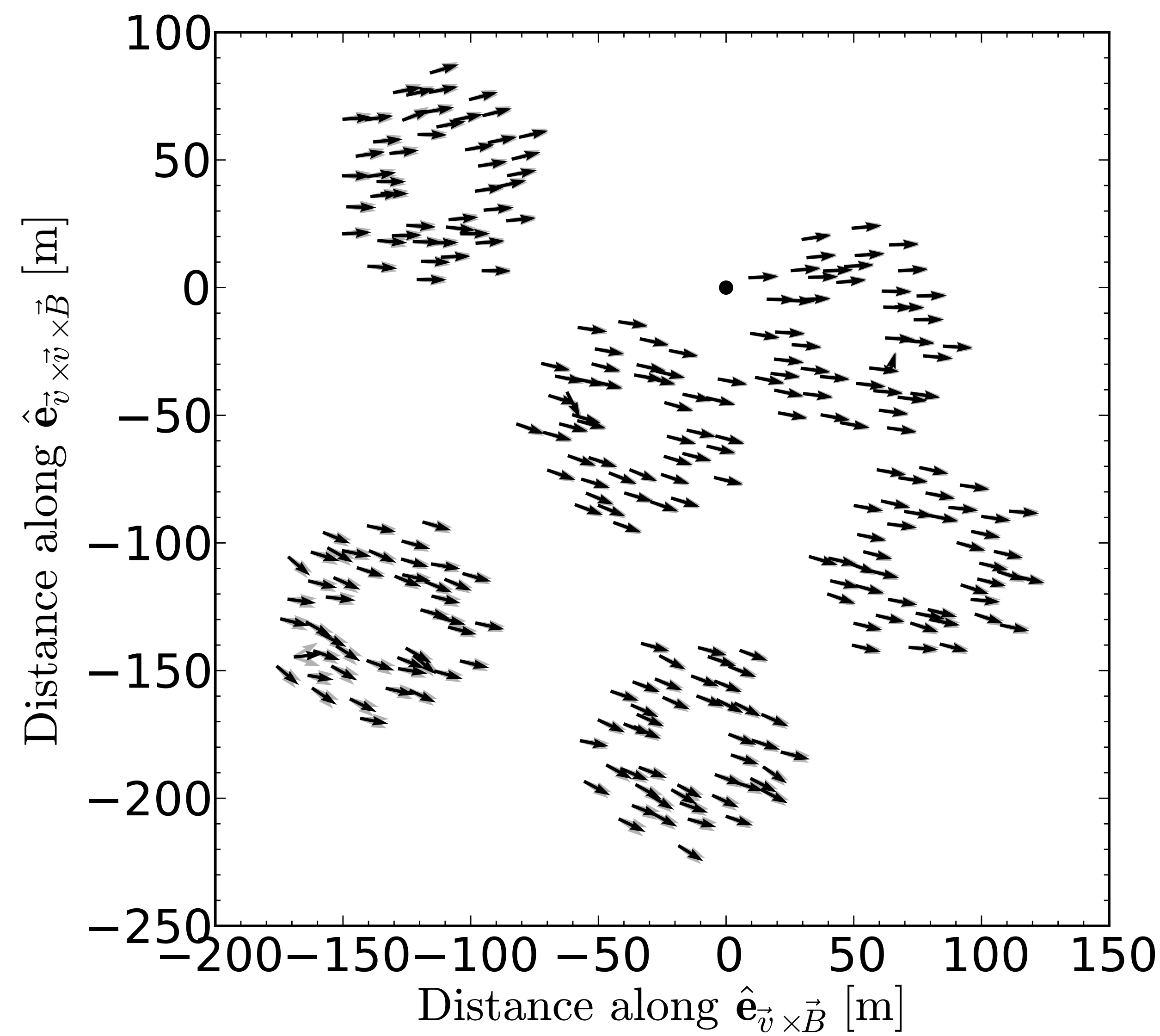

P. Schellart et al., JCAP 10 (2014) 014

Charge excess fraction

Askaryan / geomagnetic

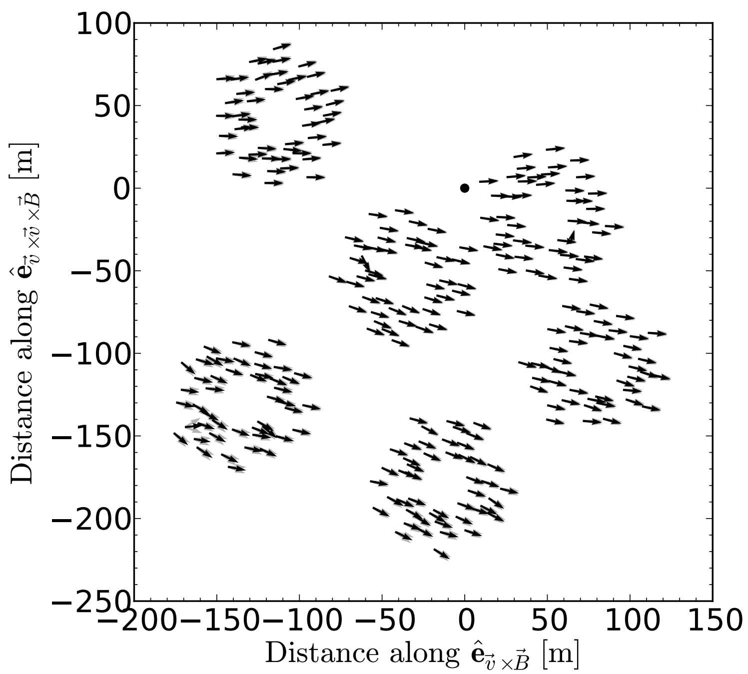

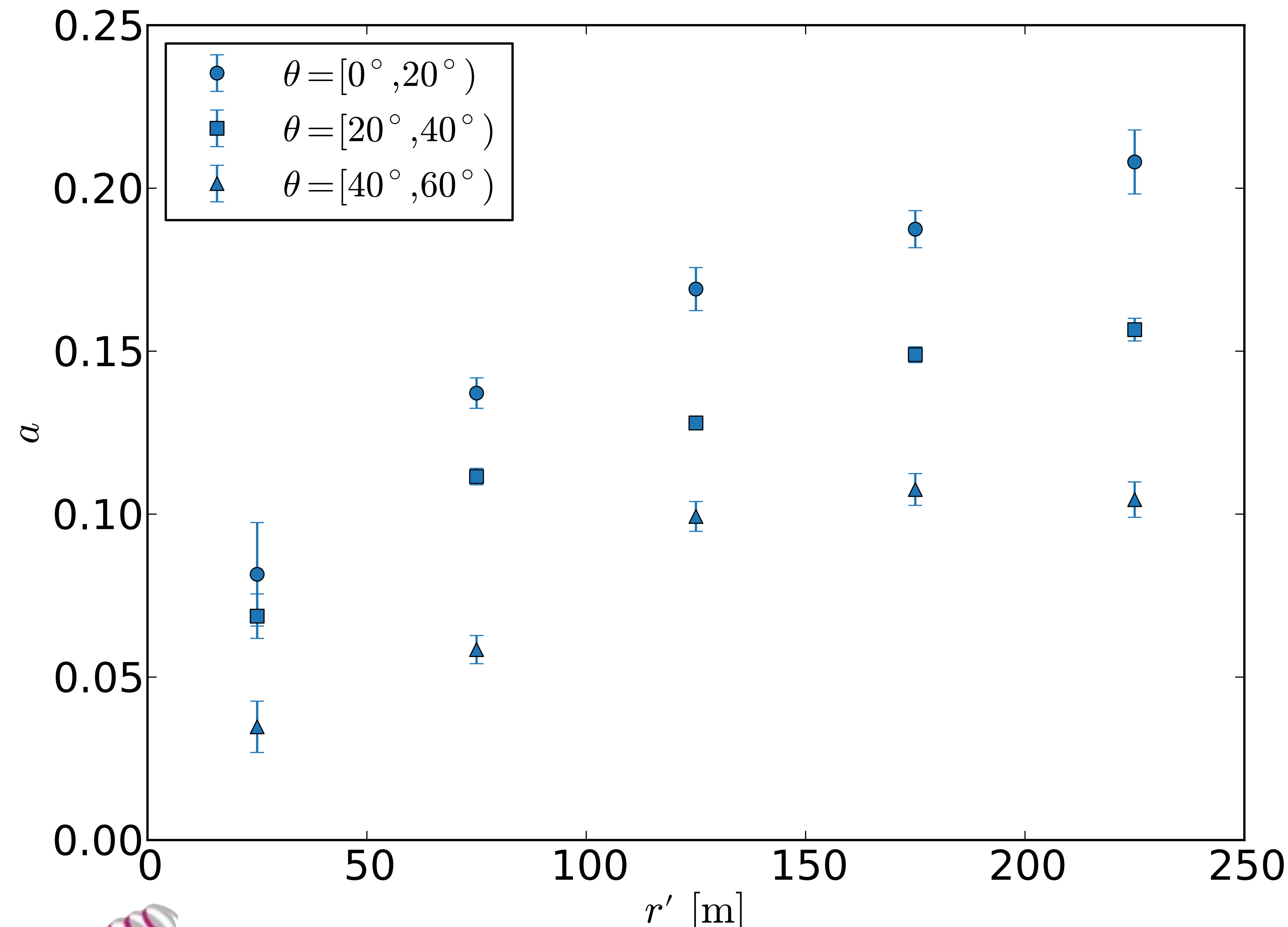

LOFAR

geomagnetic

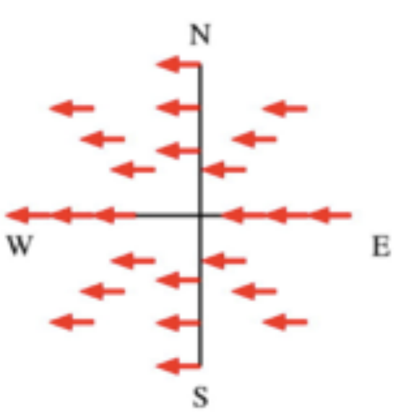

Askaryan

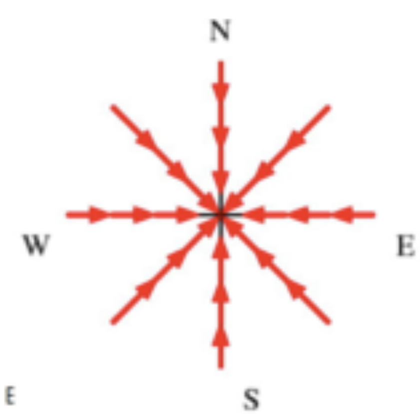

P. Schellart et al., JCAP 10 (2014) 014

Atmospheric electric fields during thunderstorms

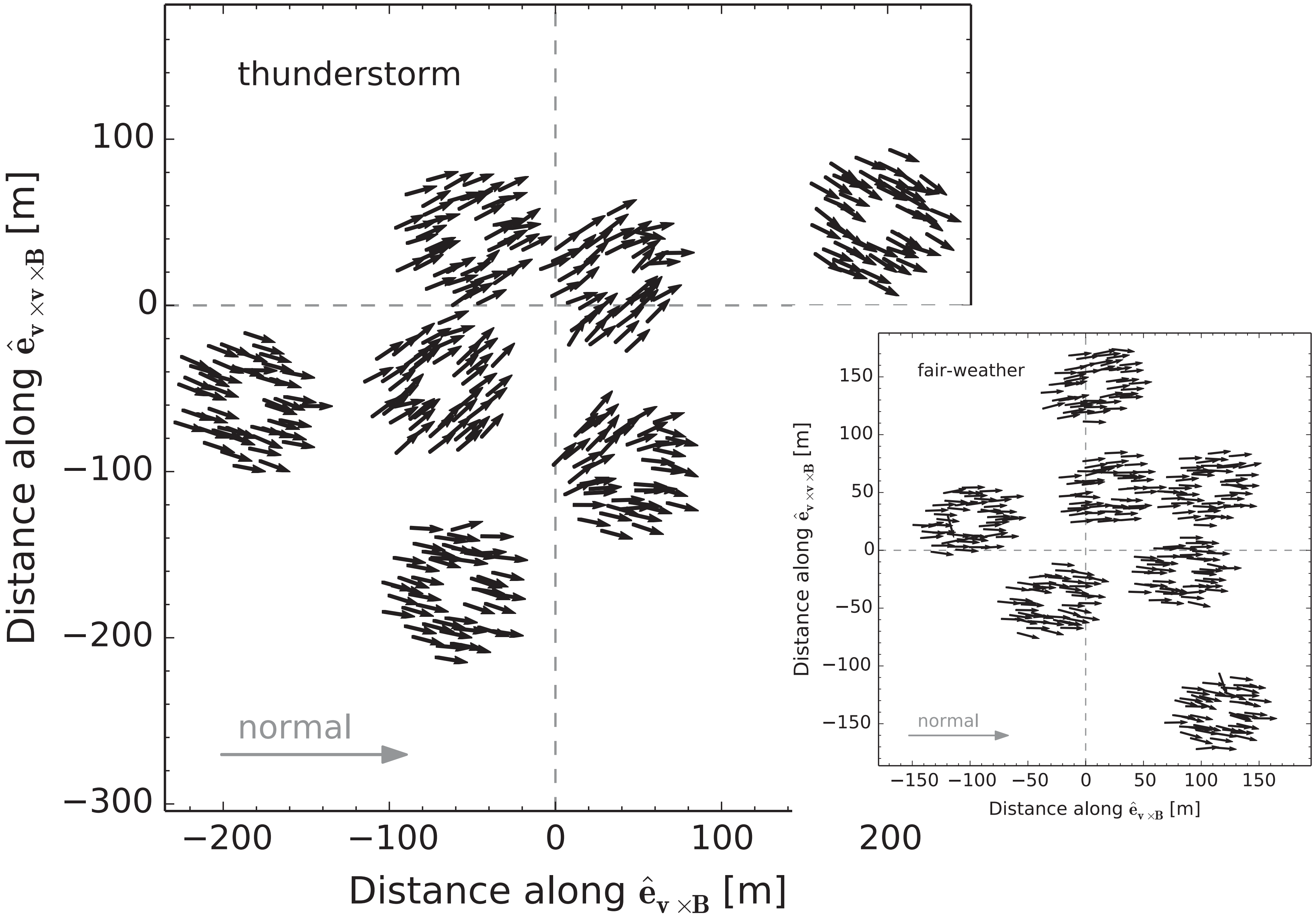

T.N.G. Trinh et al., Phys. Rev. D 93 (2016) 023003

P. Schellart et al., PRL 114 (2015) 165

Atmospheric electric fields during thunderstorms

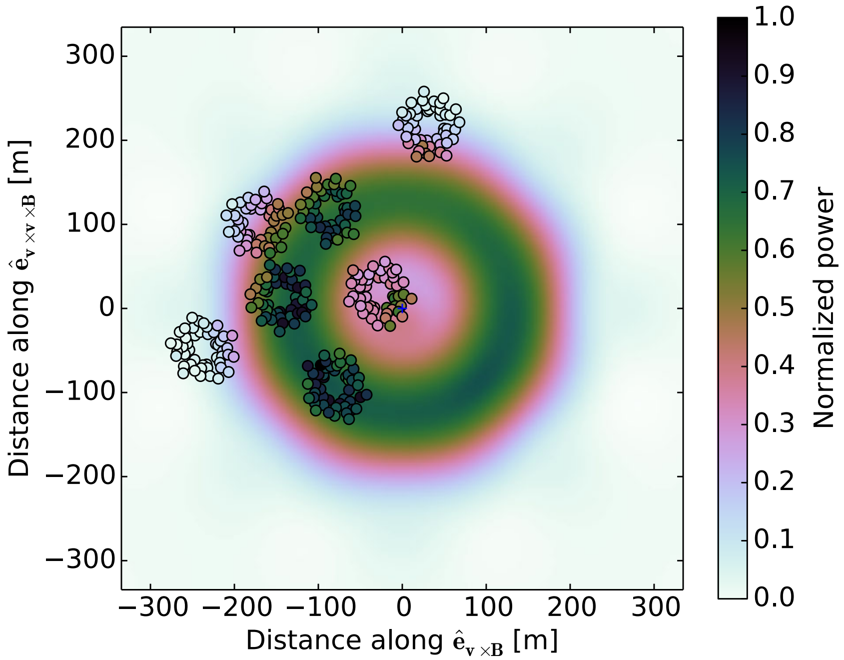

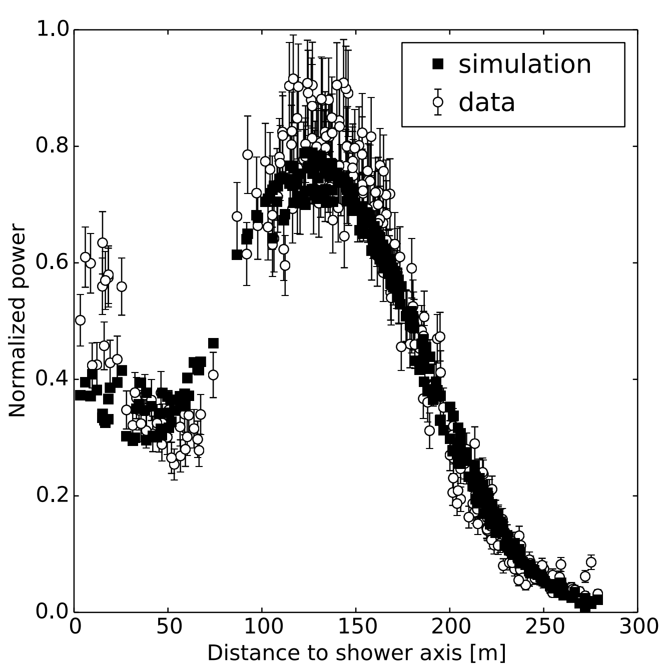

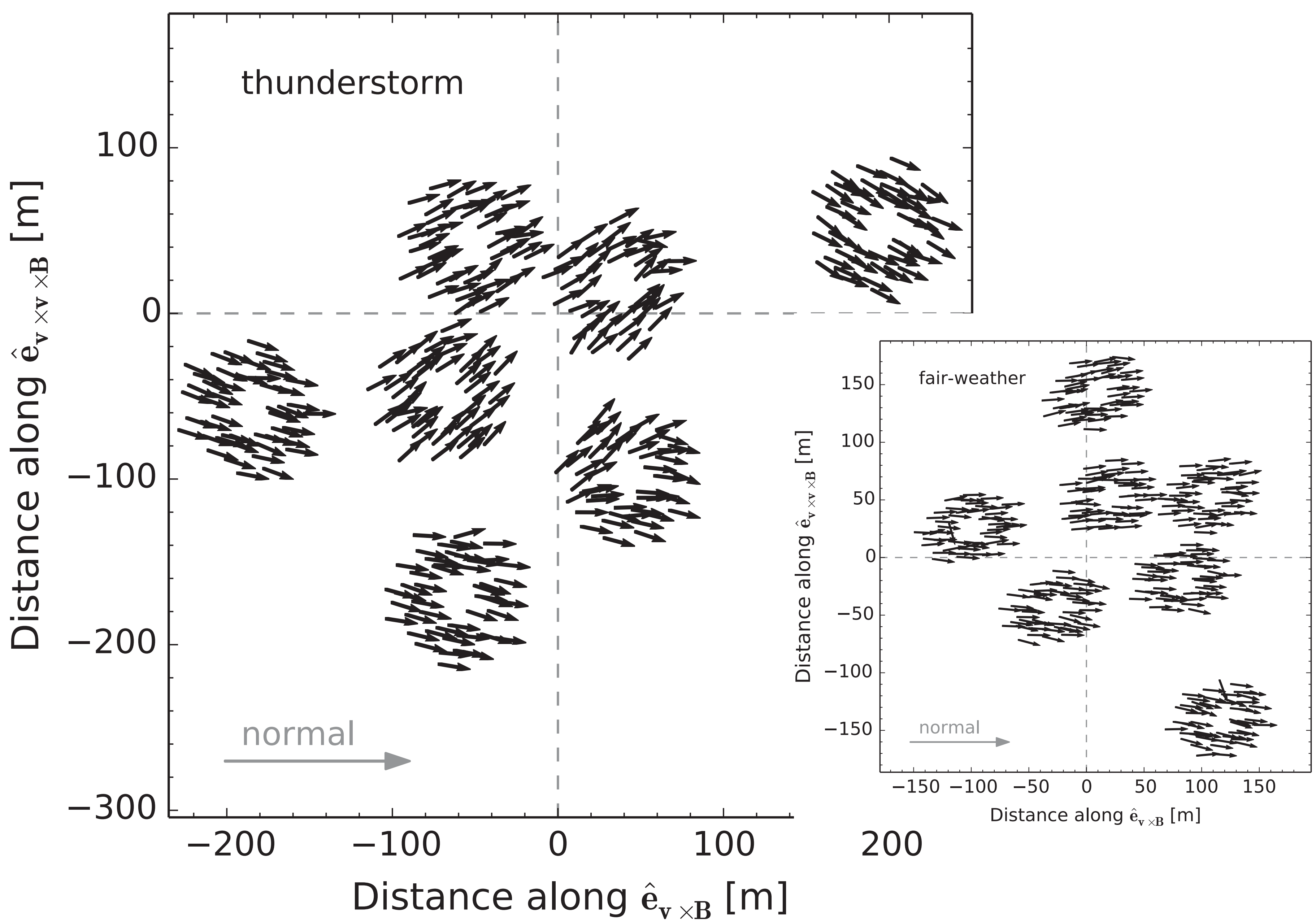

P. Schellart et al., PRL 114 (2015) 165001

Atmospheric electric fields during thunderstorms

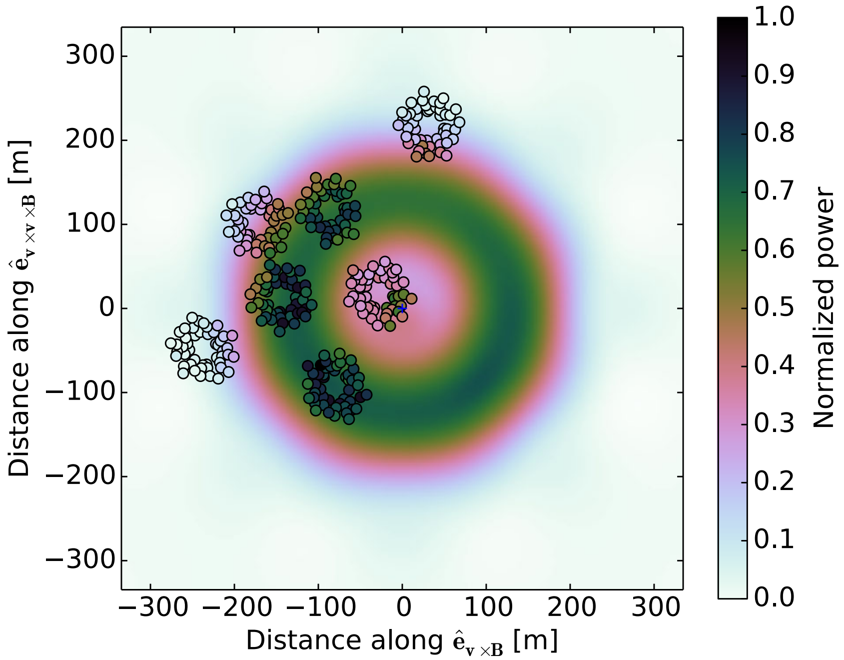

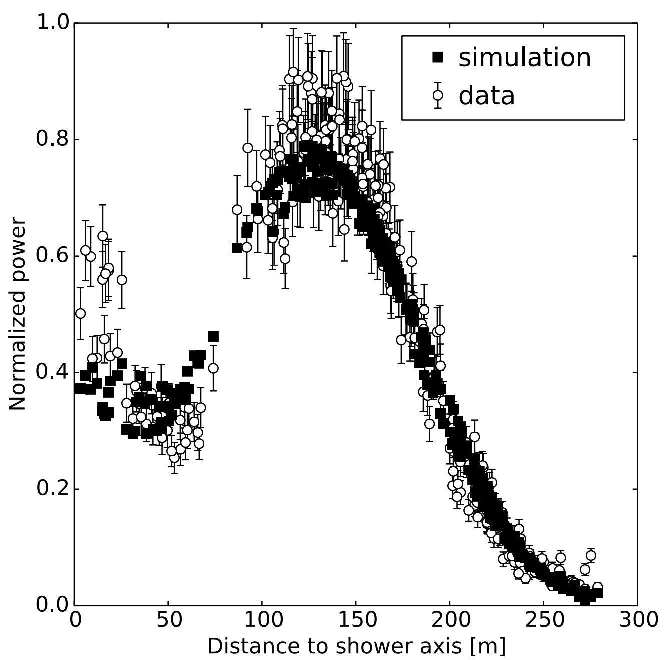

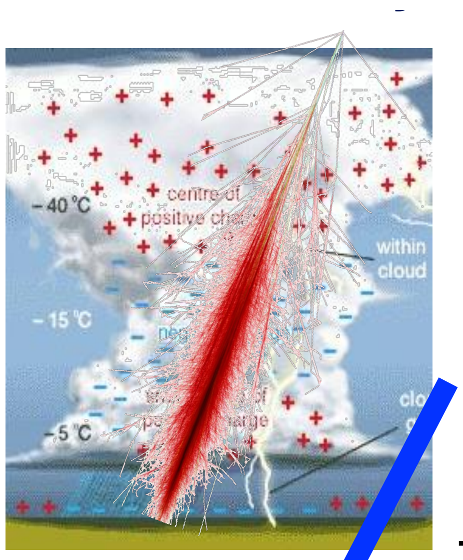

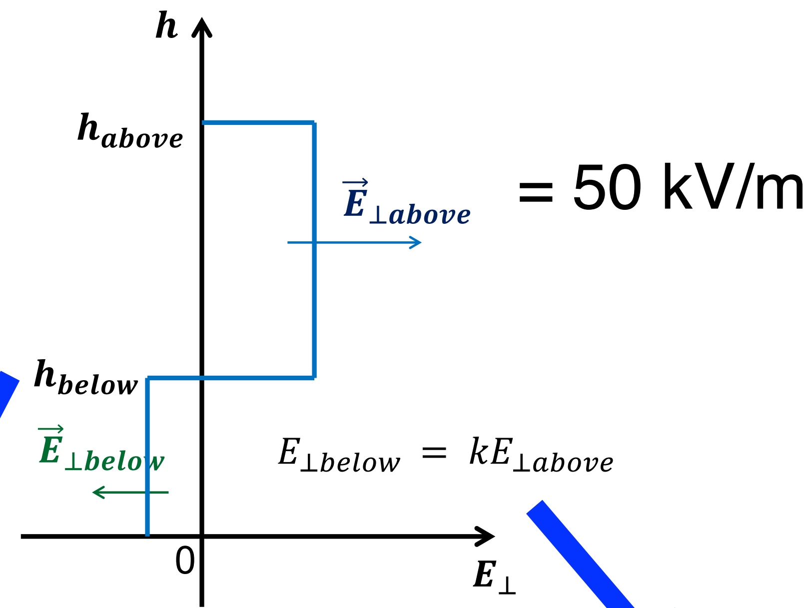

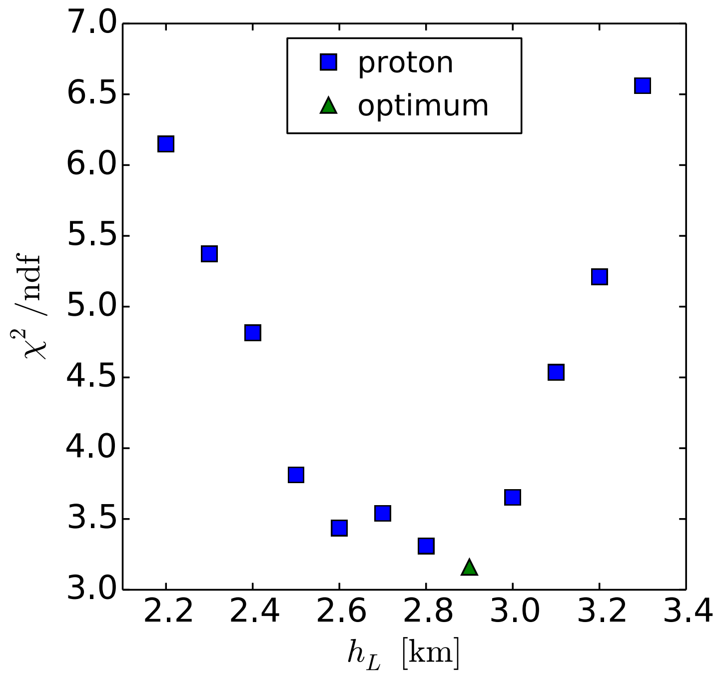

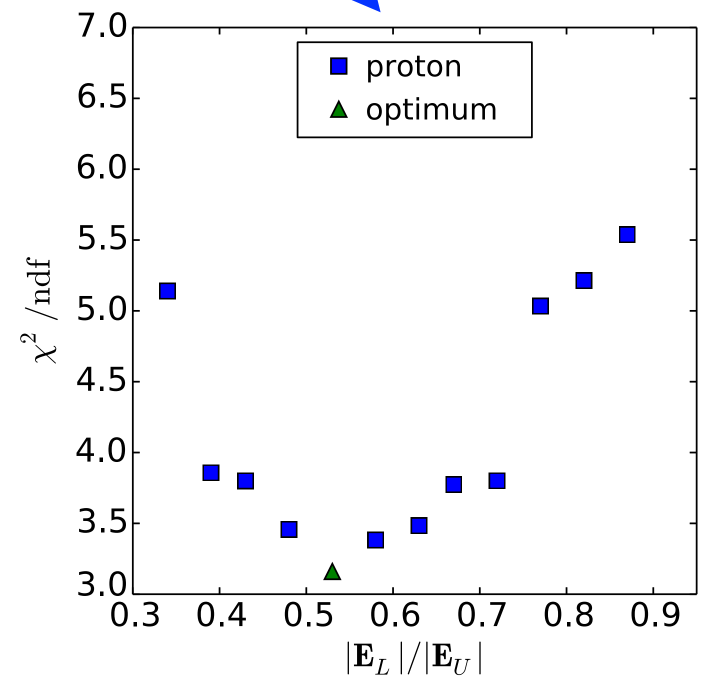

T.N.G. Trinh et al., Phys. Rev. D 93 (2016) 023003

P. Schellart et al., PRL 114 (2015) 1650

Lateral distribution of radio signals

as measured by LOFAR

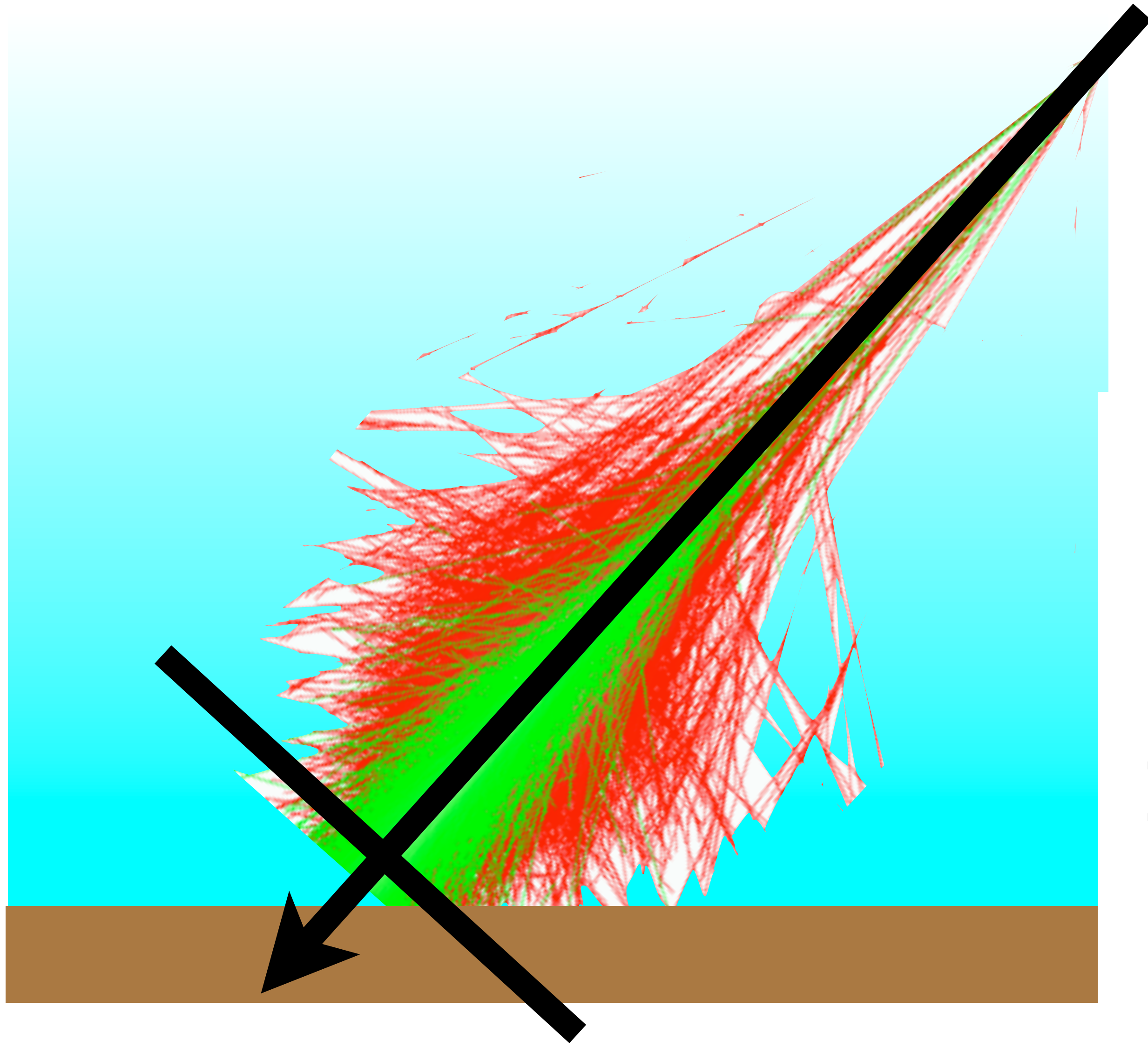

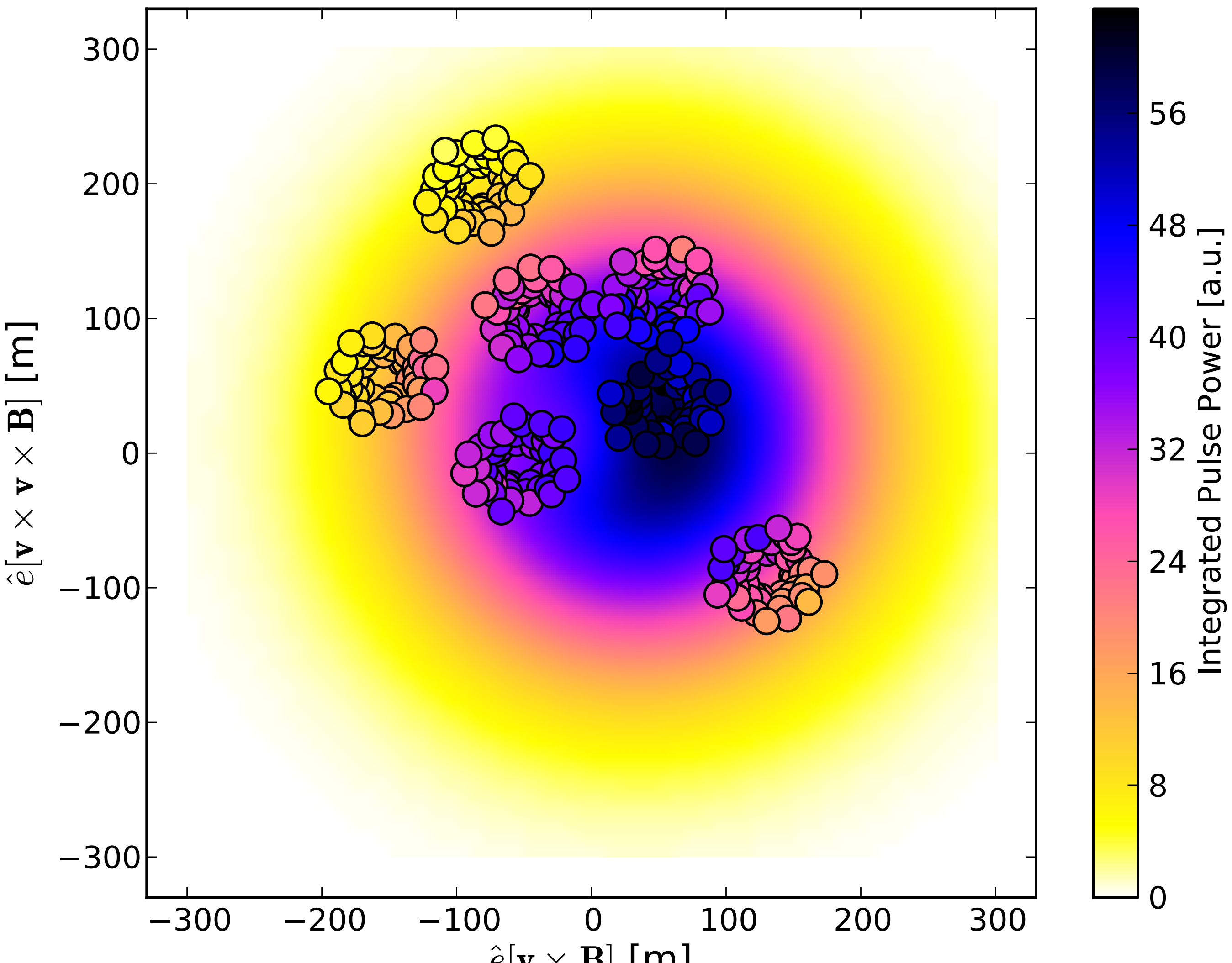

A. Nelles et al., Astropart. Phys. 60 (2015) 1

Lateral distribution of radio signals

as measured by LOFAR

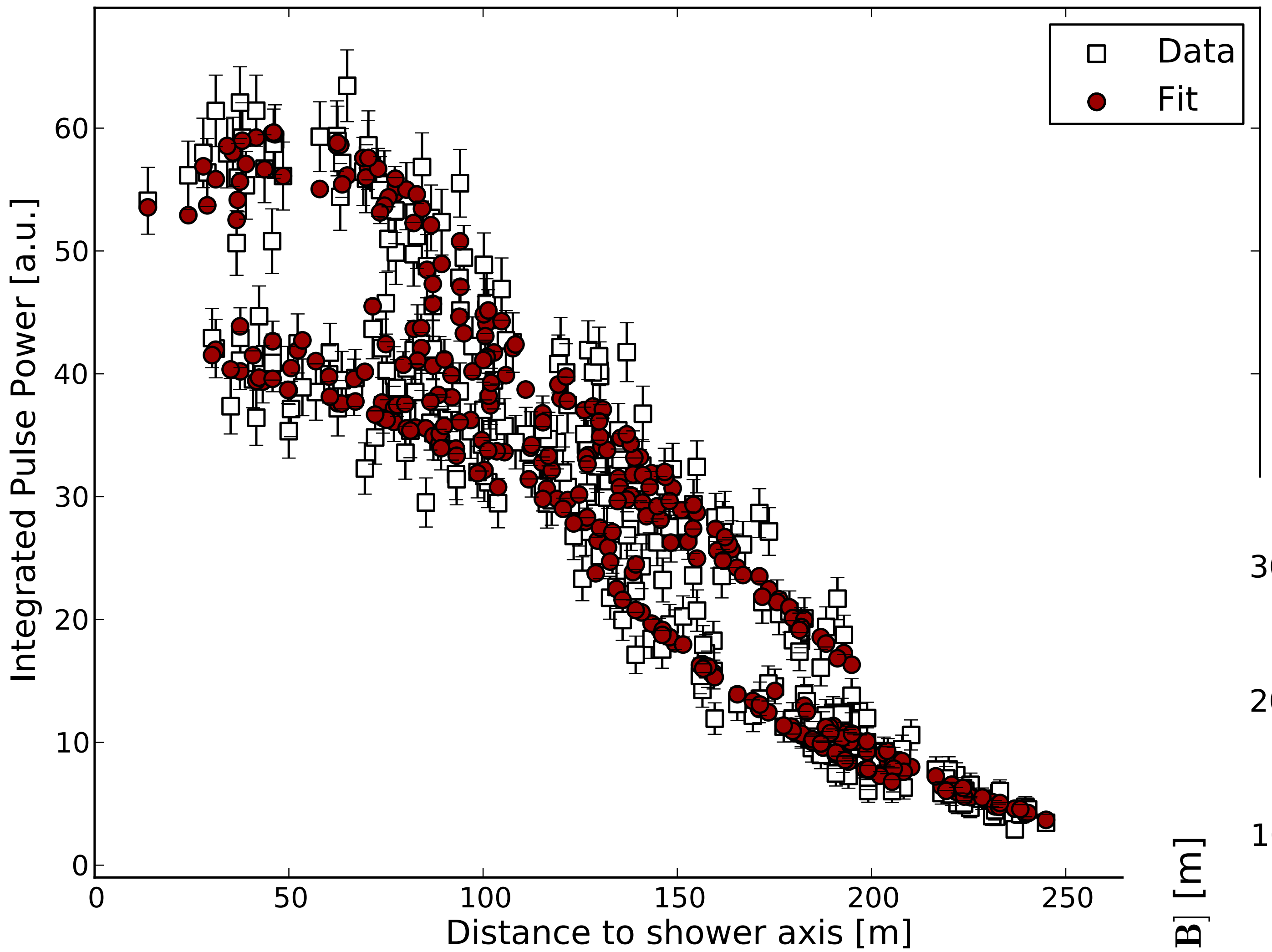

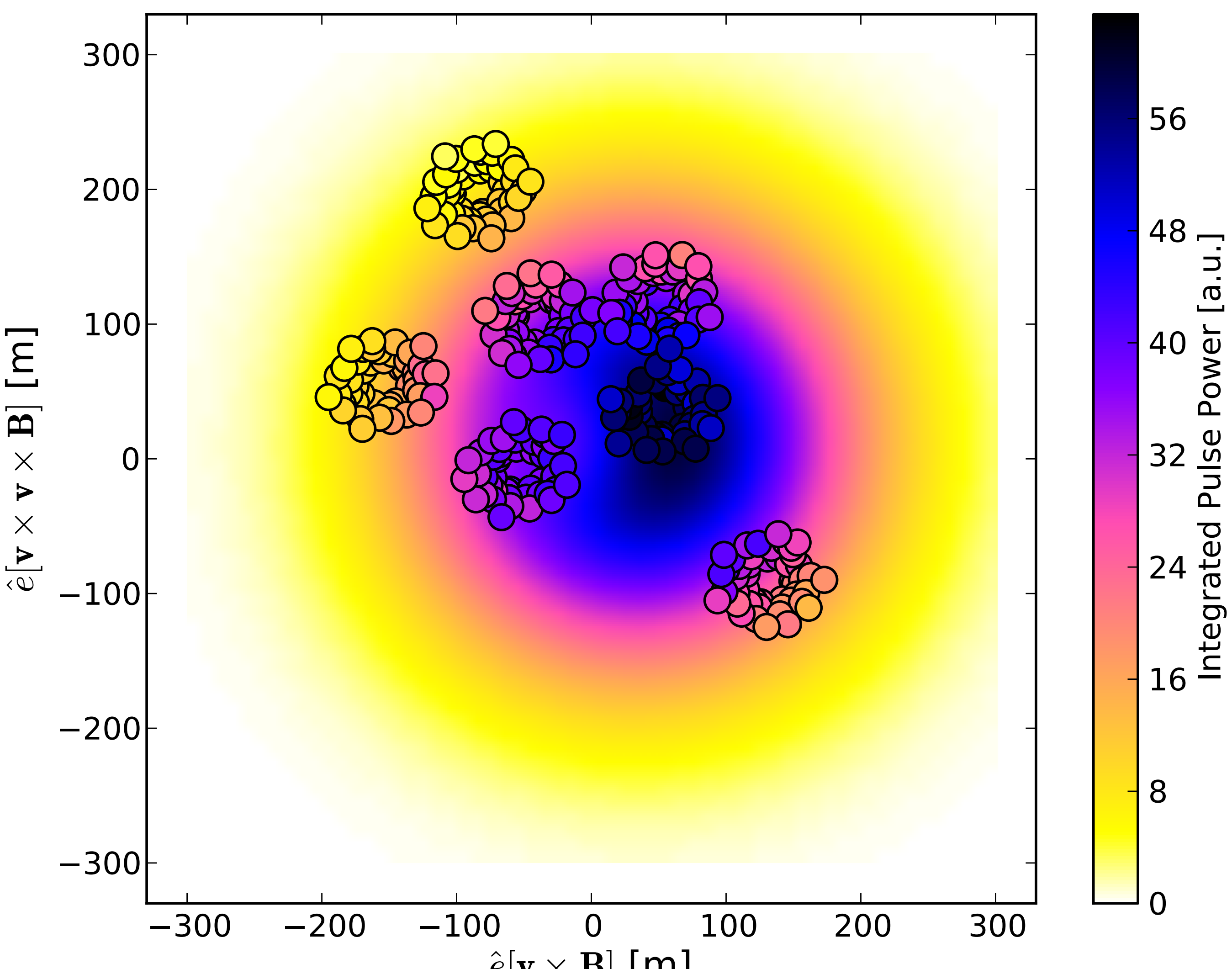

A. Nelles et al., Astropart. Phys. 60 (2015) 13

Lateral distribution of radio signals

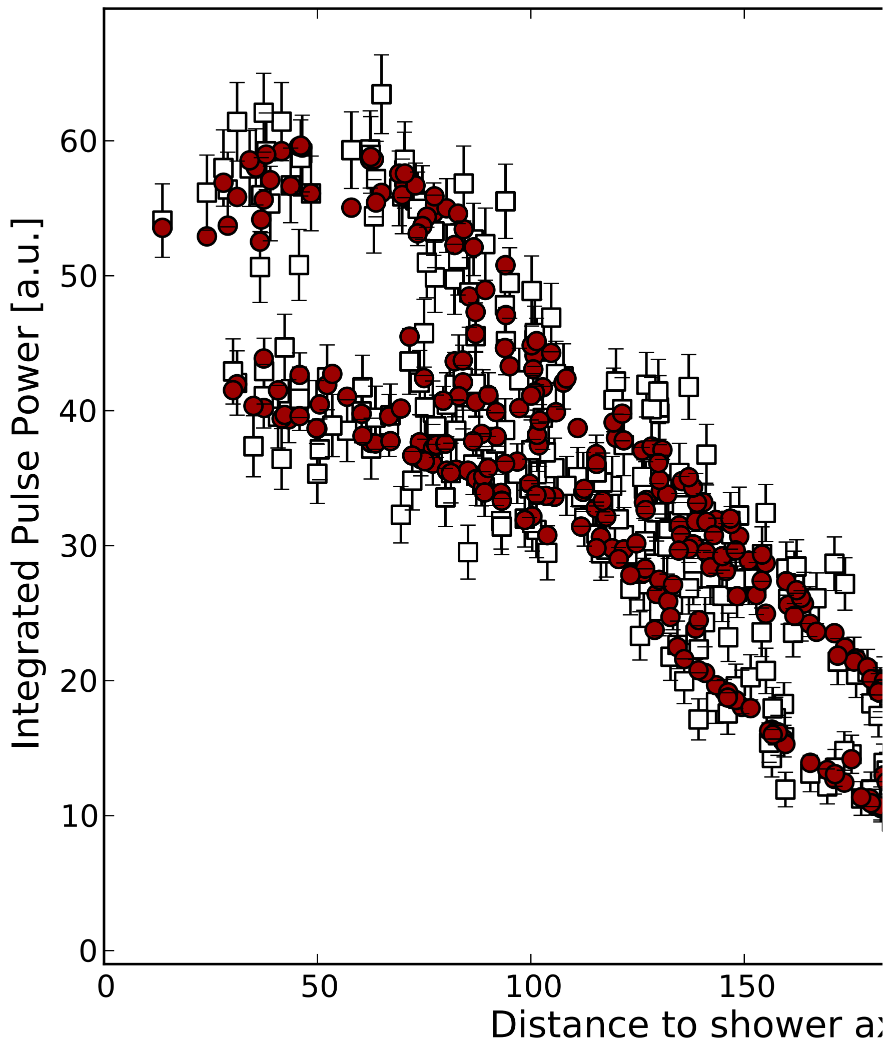

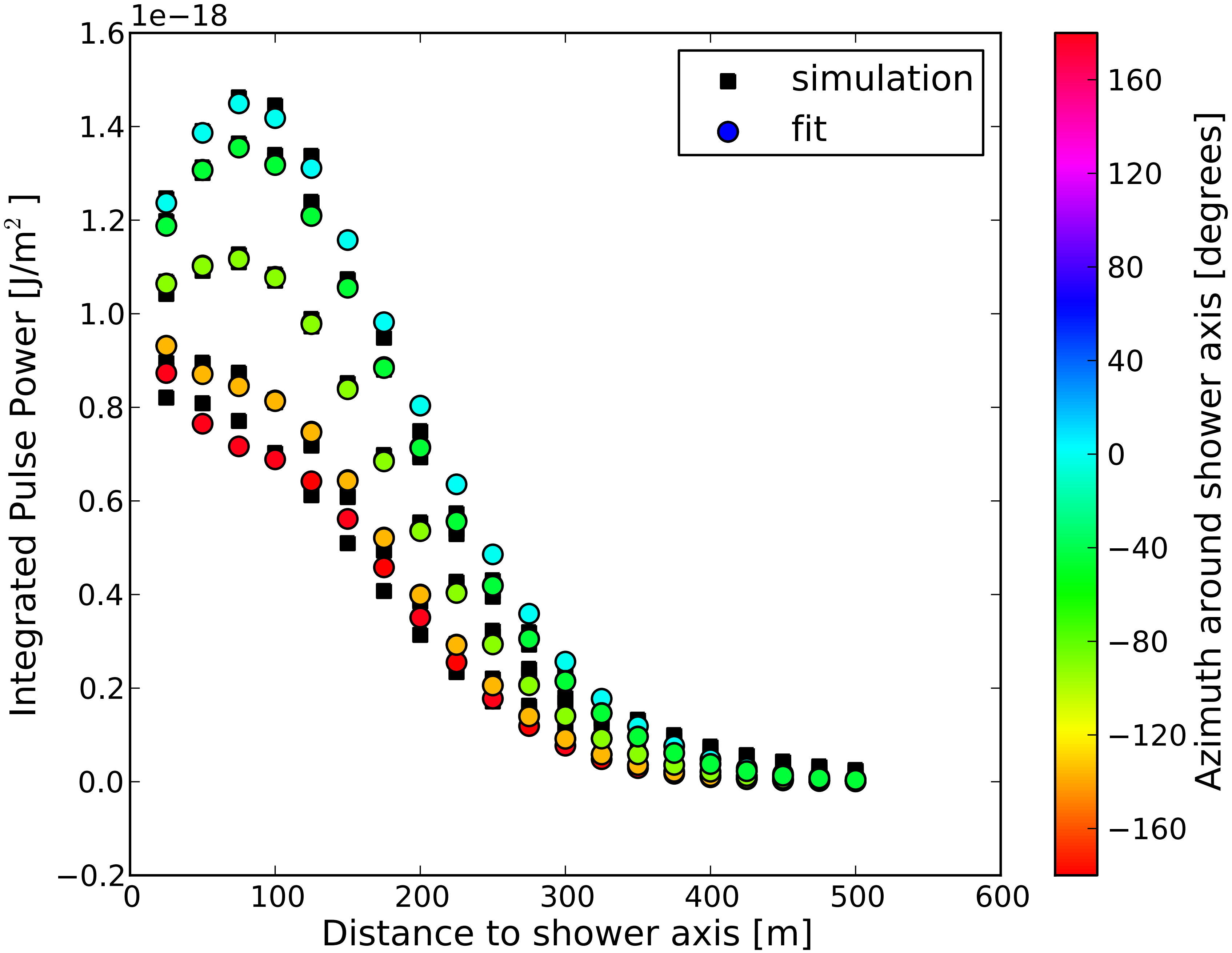

Lateral distribution of radio signals

not rotationally symmetric

fit two Gaussian functions

$$P(x',y') = A_+ \cdot \exp\left(\frac{-[(x'-X_+)^2+(y'-Y_+)^2]}{\sigma_+^2}\right) - A_- \cdot \exp\left(\frac{-[(x'-X_-)^2+(y'-Y_-)^2]}{\sigma_-^2}\right) + O$$

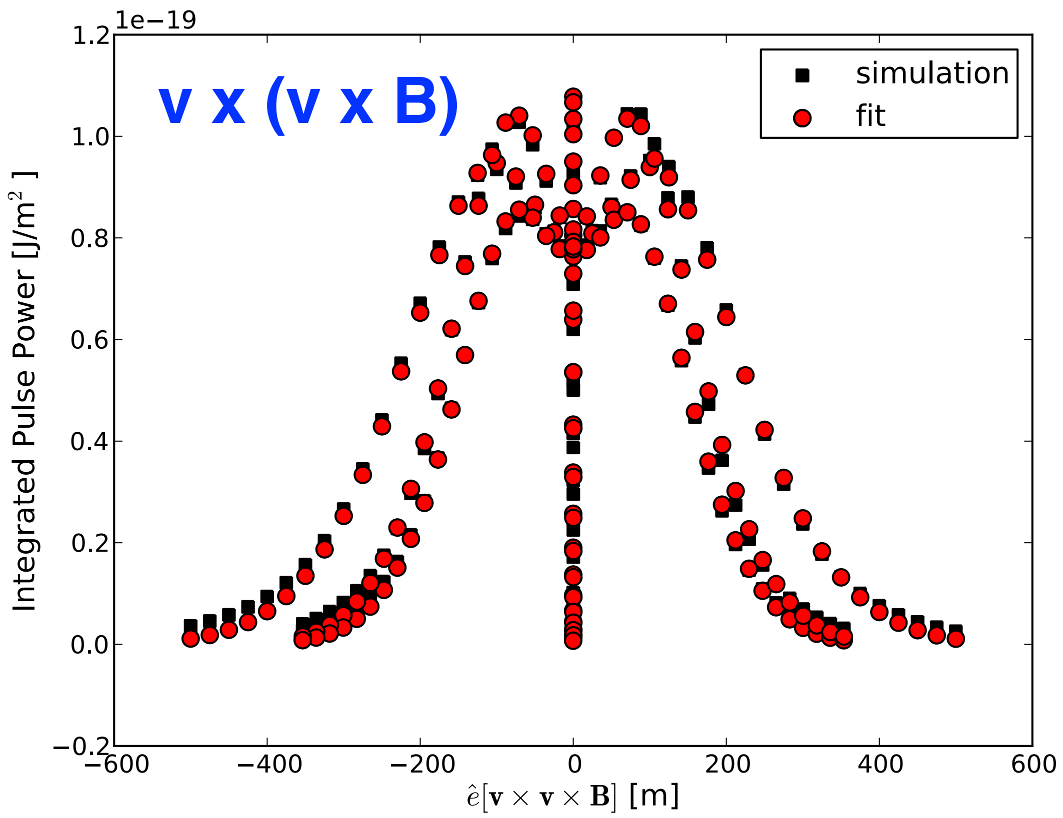

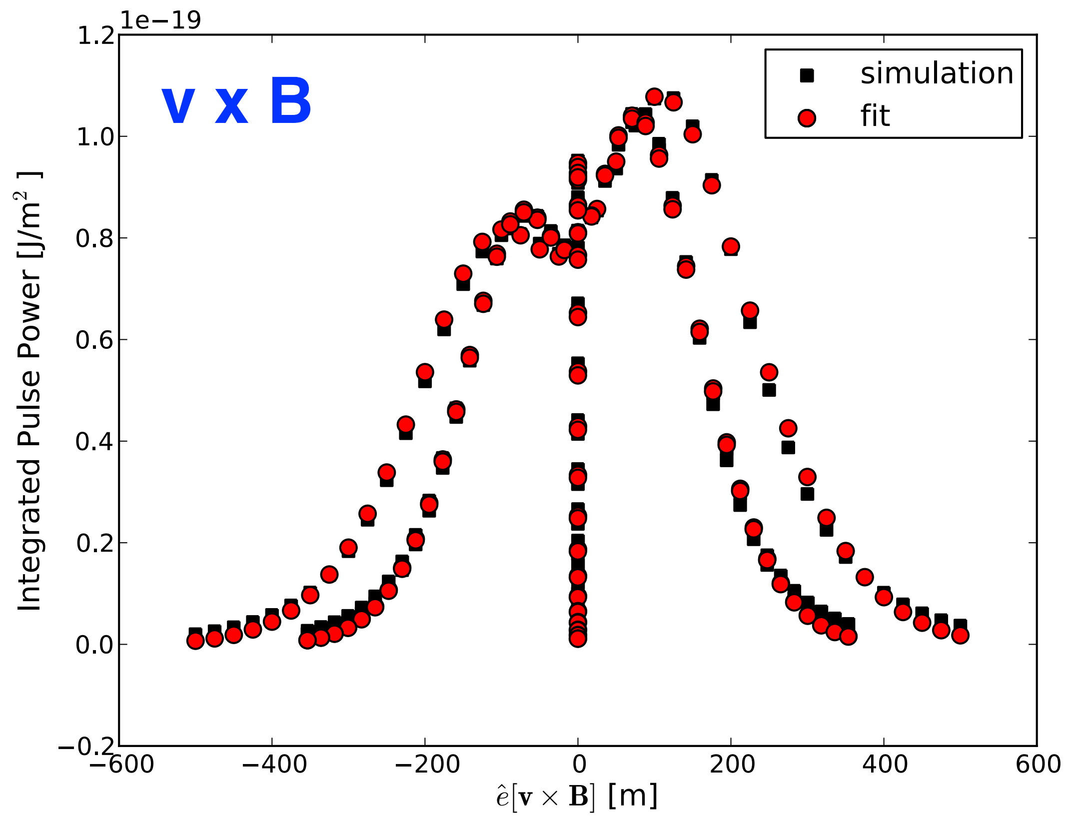

A. Nelles et al., Astropart. Phys. 60 (2015) 13

Measuring Cherenkov Rings

110 - 190 MHz

- **LOFAR is the only dedicated experiment with high-band antennas**
- **higher frequency-range: dominance of relativistic time-compression**
- **signals expected to be on a ring of emission**
- **first experiment to observe these in single showers**

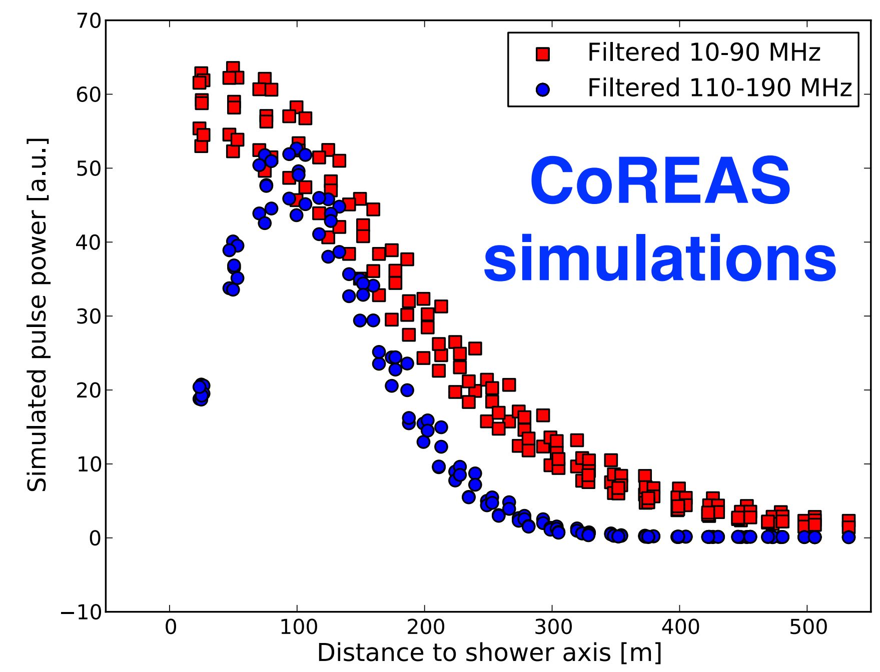

A. Nelles et al., Astroparticle Physics 65 (2015) 11

Measuring Cherenkov Rings

110 - 190 MHz

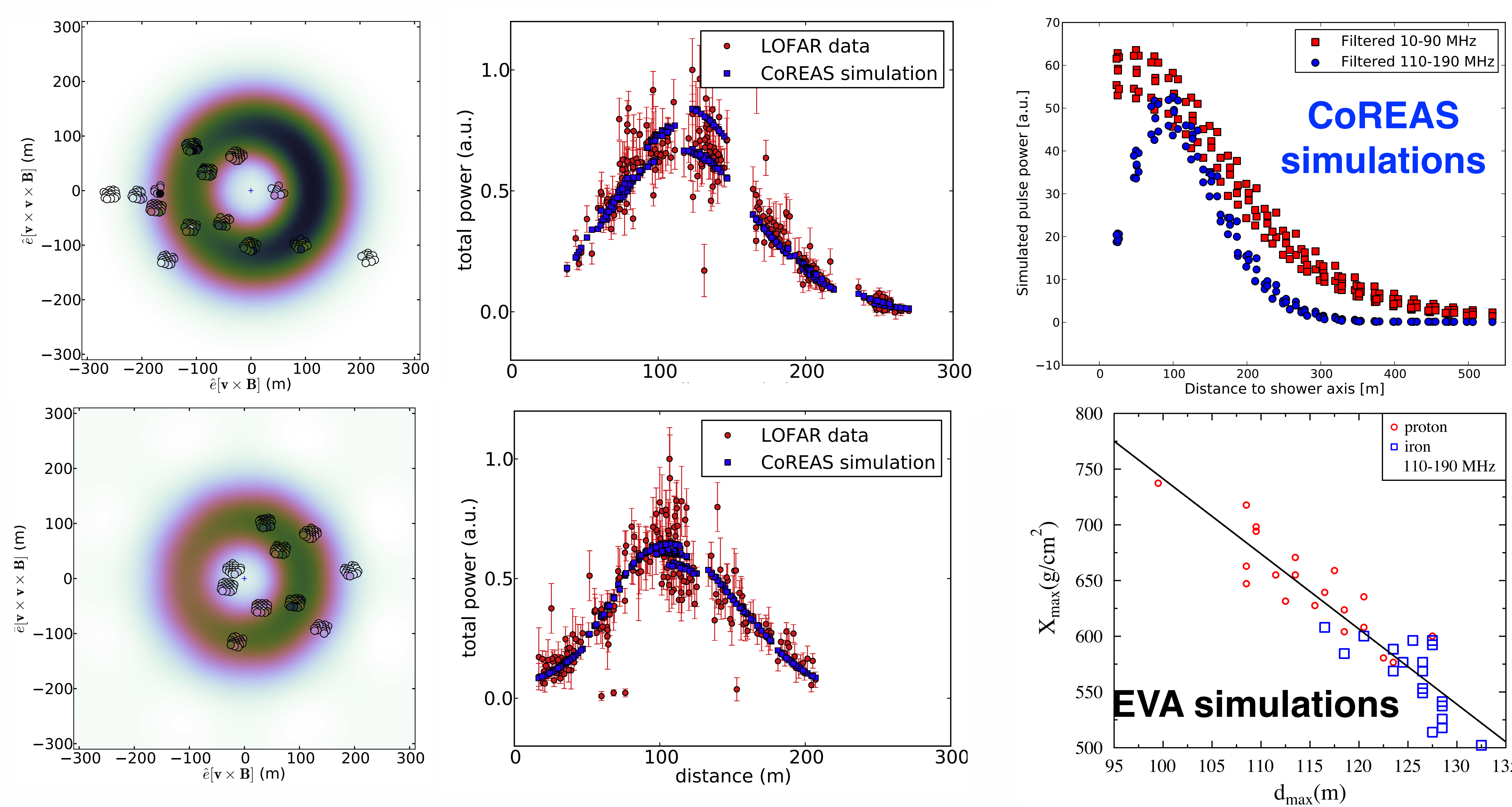

ring size sensitive to Xmax

A. Nelles et al., Astroparticle Physics 65 (2015) 11

Shape of the Shower Front

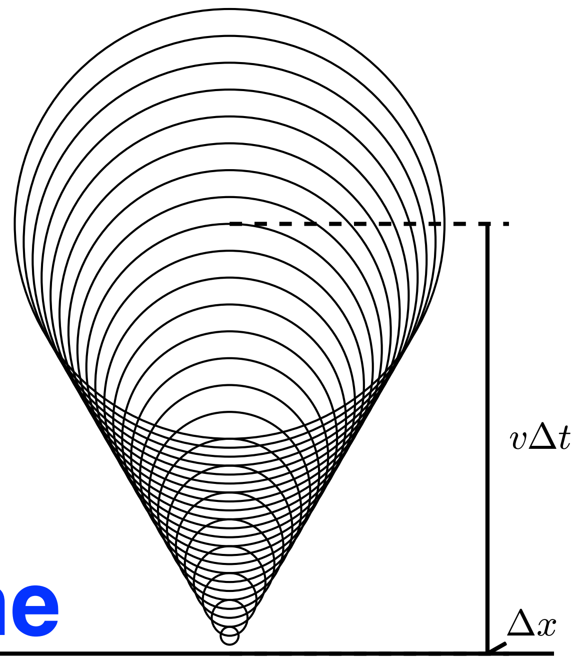

cone

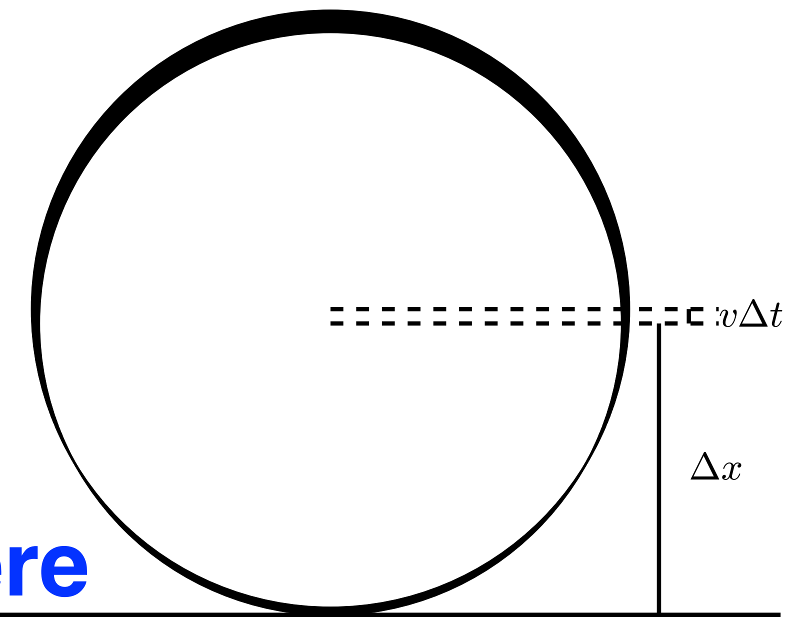

sphere

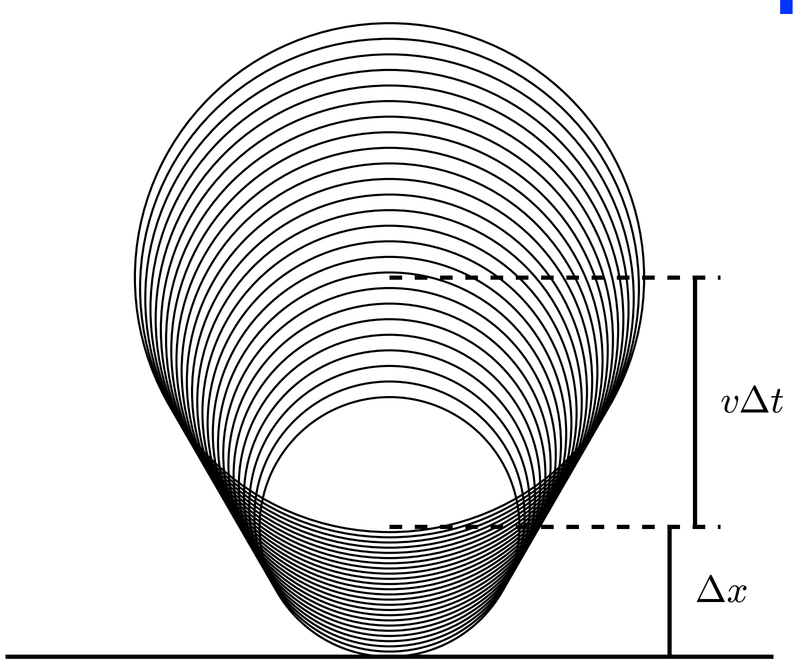

hyperboloid

Shape of Shower Front

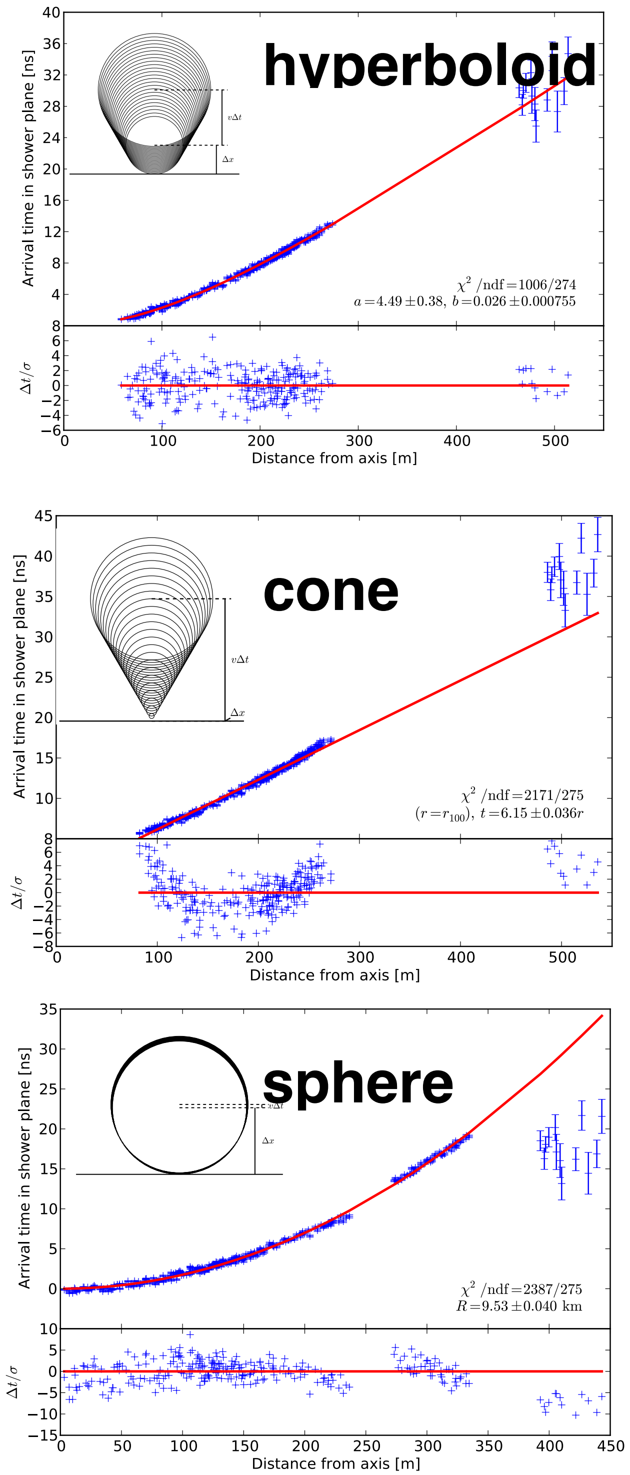

fit quality

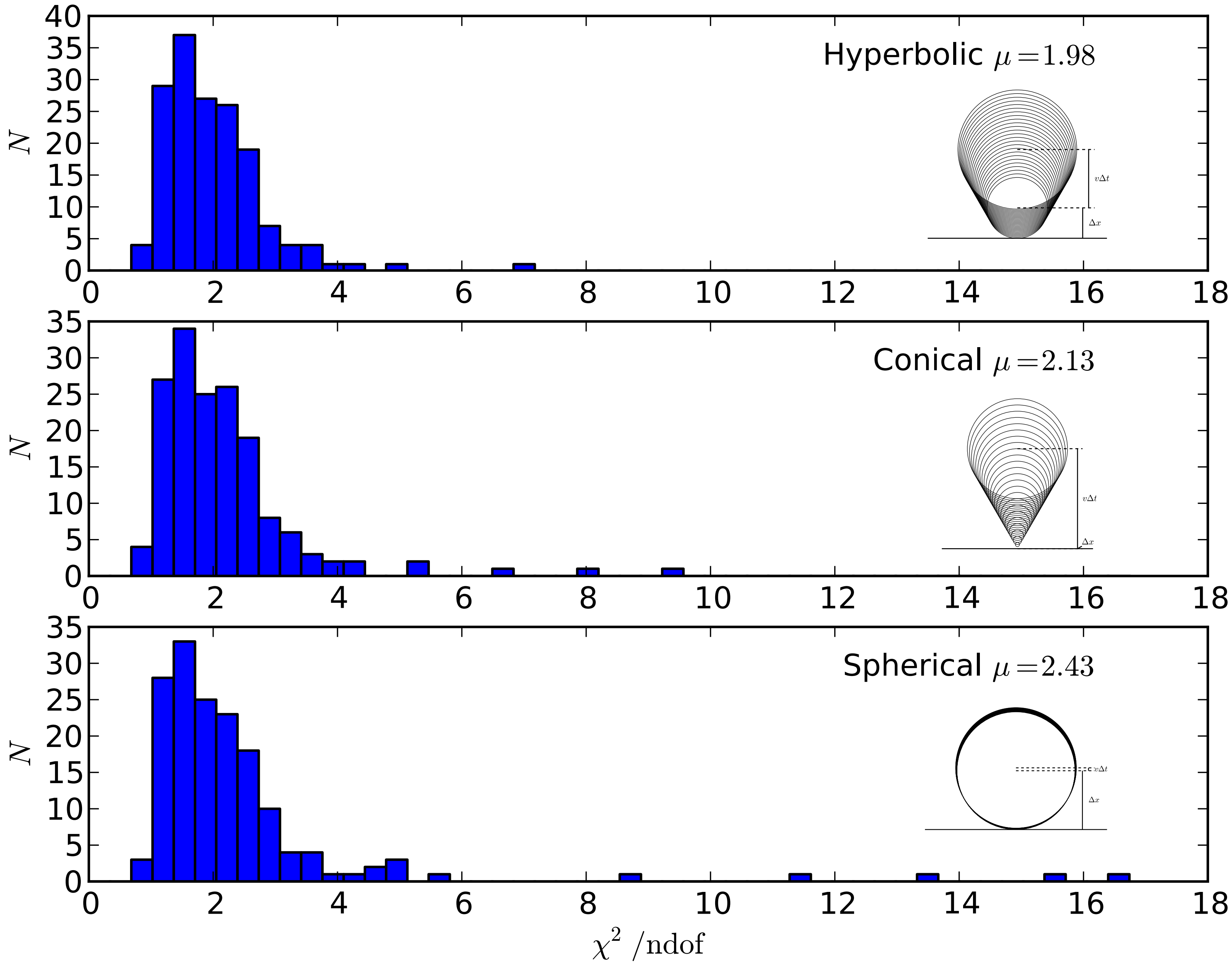

A. Corstanje et al., Astropart. Phys. 61 (2015) 22

Accuracy of Shower Direction

angular difference between..

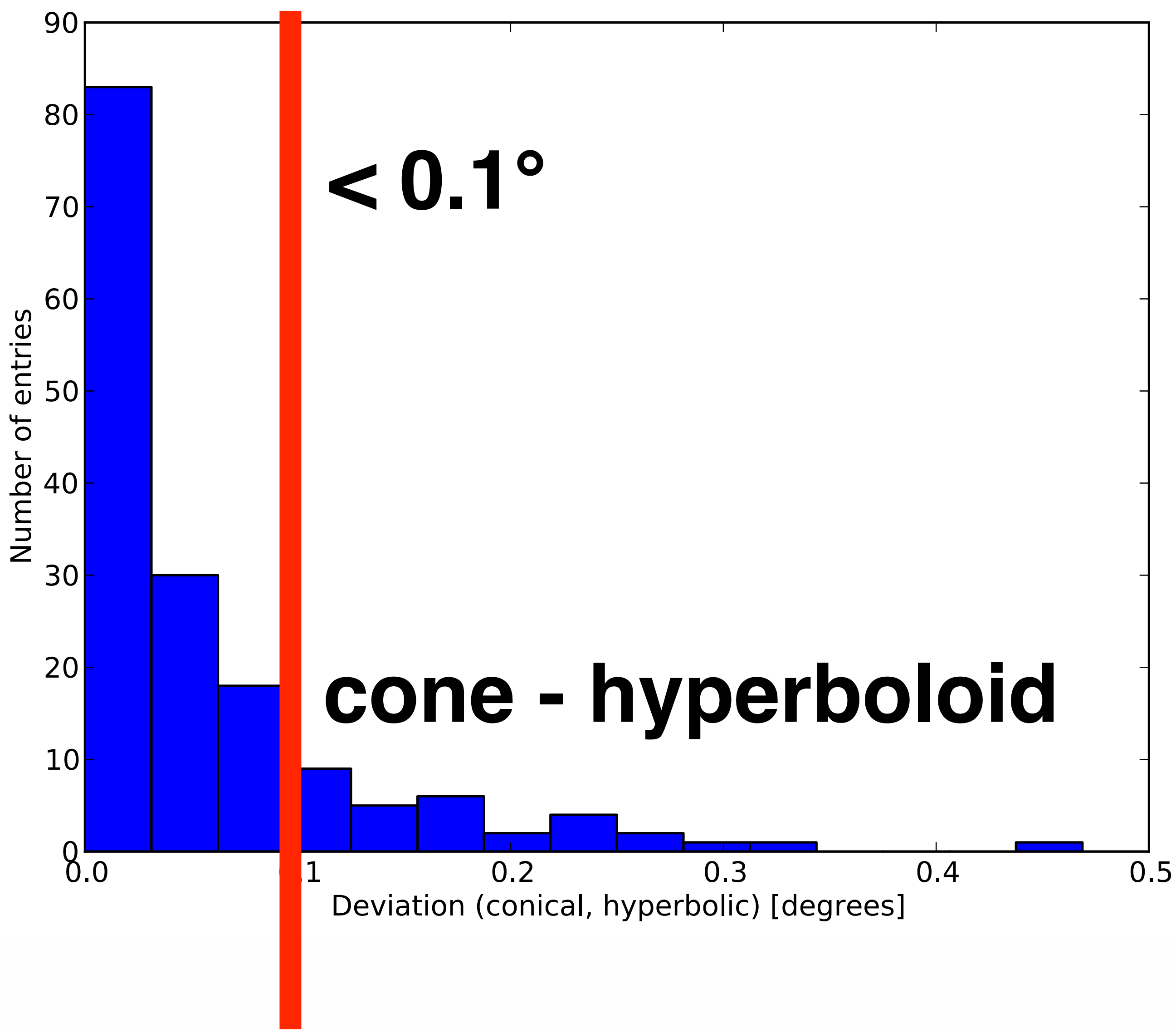

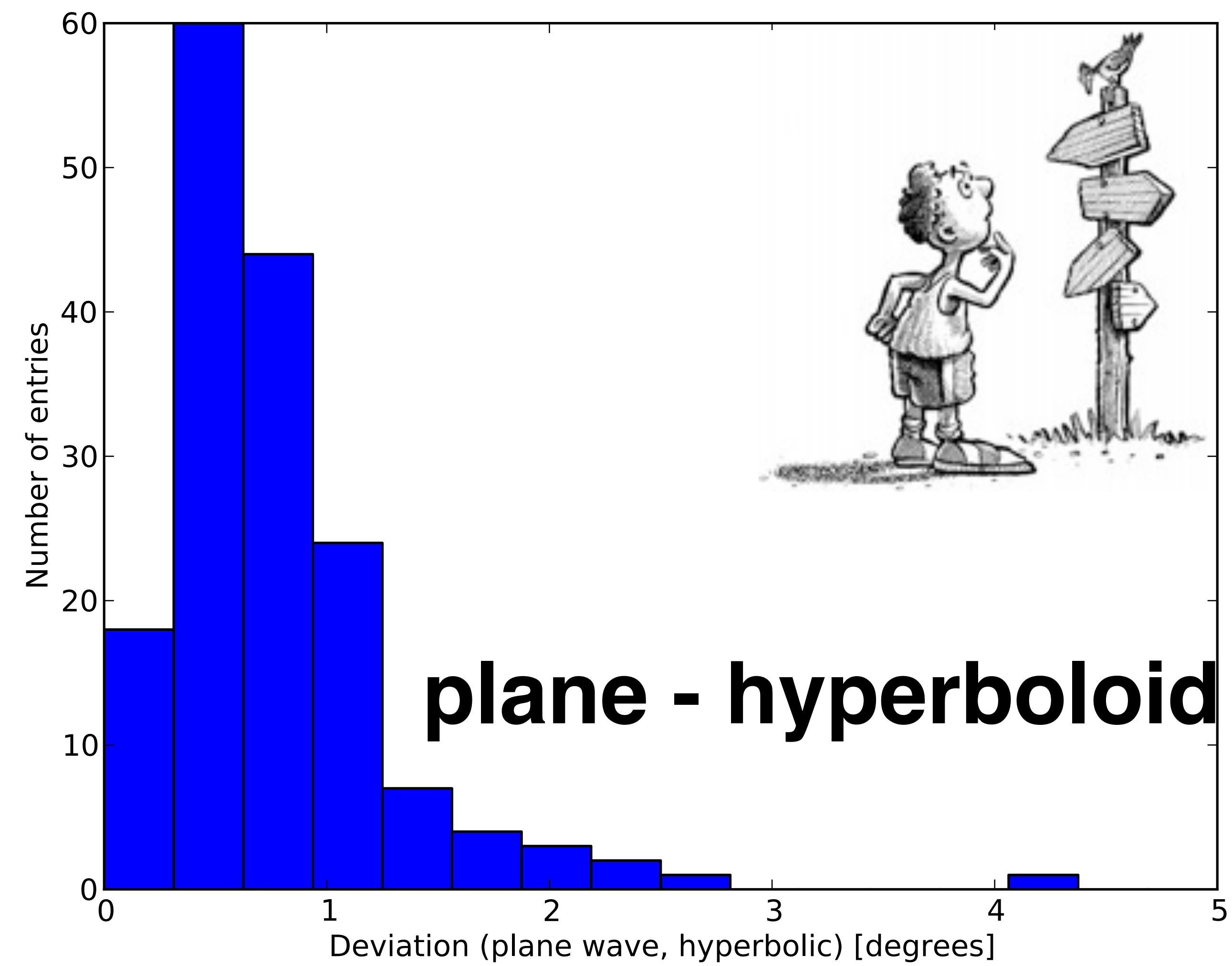

A. Corstanje et al., Astropart. Phys. 61 (2015) 22

LOFAR

Energy of primary particle

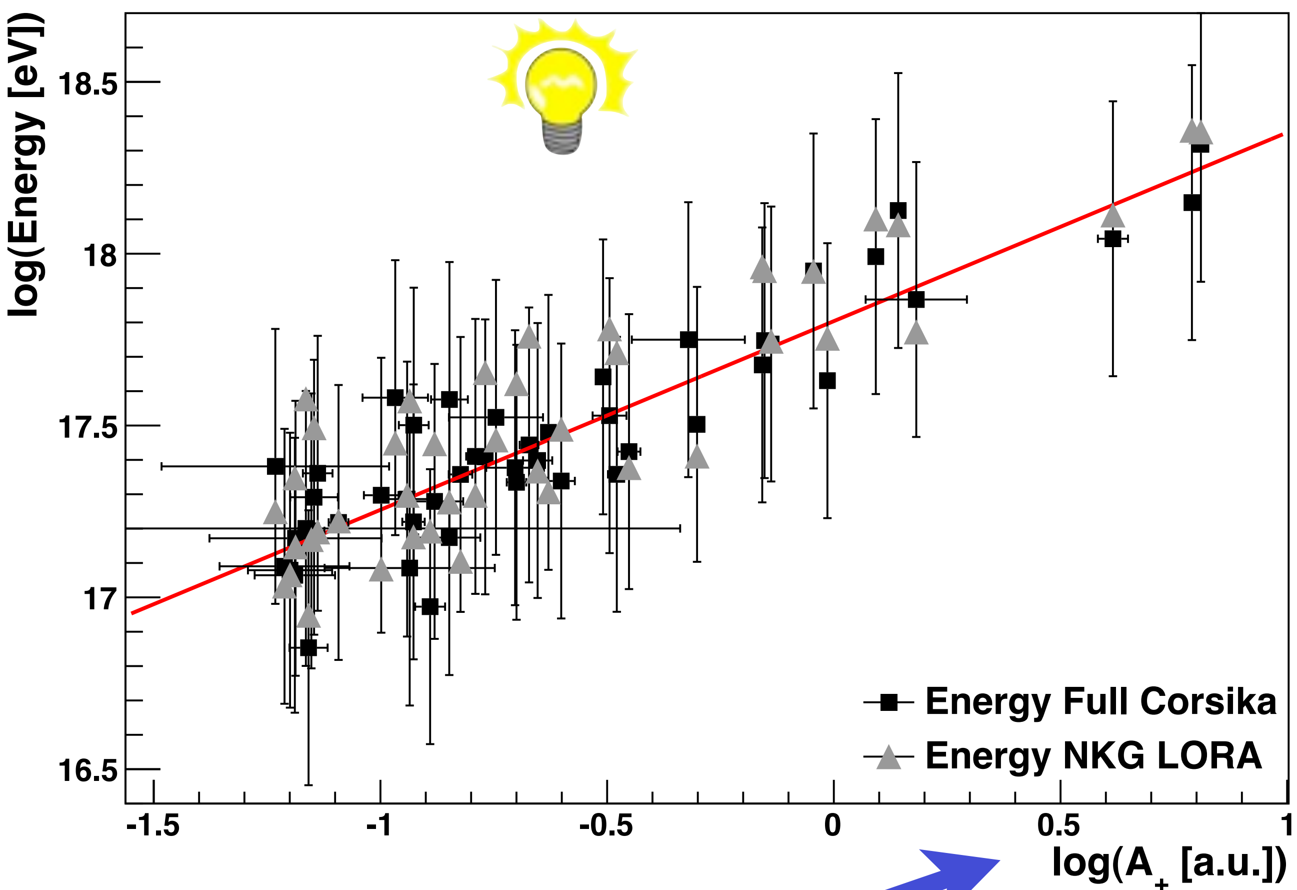

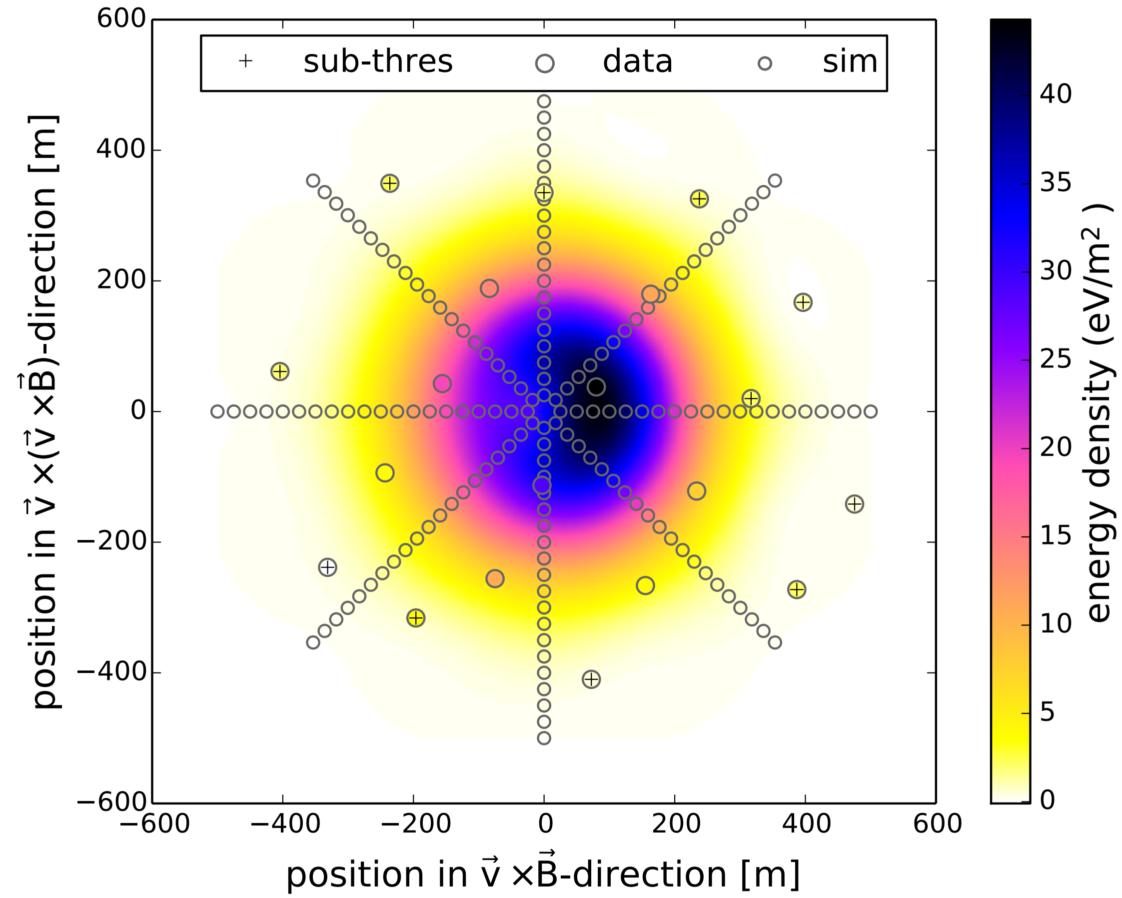

$$P(x', y') = A_+ \cdot \exp\left(\frac{-[(x' - X_+)^2 + (y' - Y_+)^2]}{\sigma_+^2}\right) - A_- \cdot \exp\left(\frac{-[(x' - X_-)^2 + (y' - Y_-)^2]}{\sigma_-^2}\right) + O$$

LOFAR

A. Nelles et al., JCAP 05 (2015) 018

Energy of primary particle

PIERRE AUGER OBSERVATORY

AERA Auger Engineering Radio Array

measurement of radio content of air shower on absolute scale

--> Florian Gaté 11:00-11:15

$$P(x', y') = A_+ \cdot \exp\left(\frac{-[(x'-X_+)^2 + (y'-Y_+)^2]}{\sigma_+^2}\right) - A_- \cdot \exp\left(\frac{-[(x'-X_-)^2 + (y'-Y_-)^2]}{\sigma_-^2}\right) + O$$

LOFAR

A. Nelles et al., JCAP 05 (2015) 018

Properties of primary particle

energy

distance to Xmax

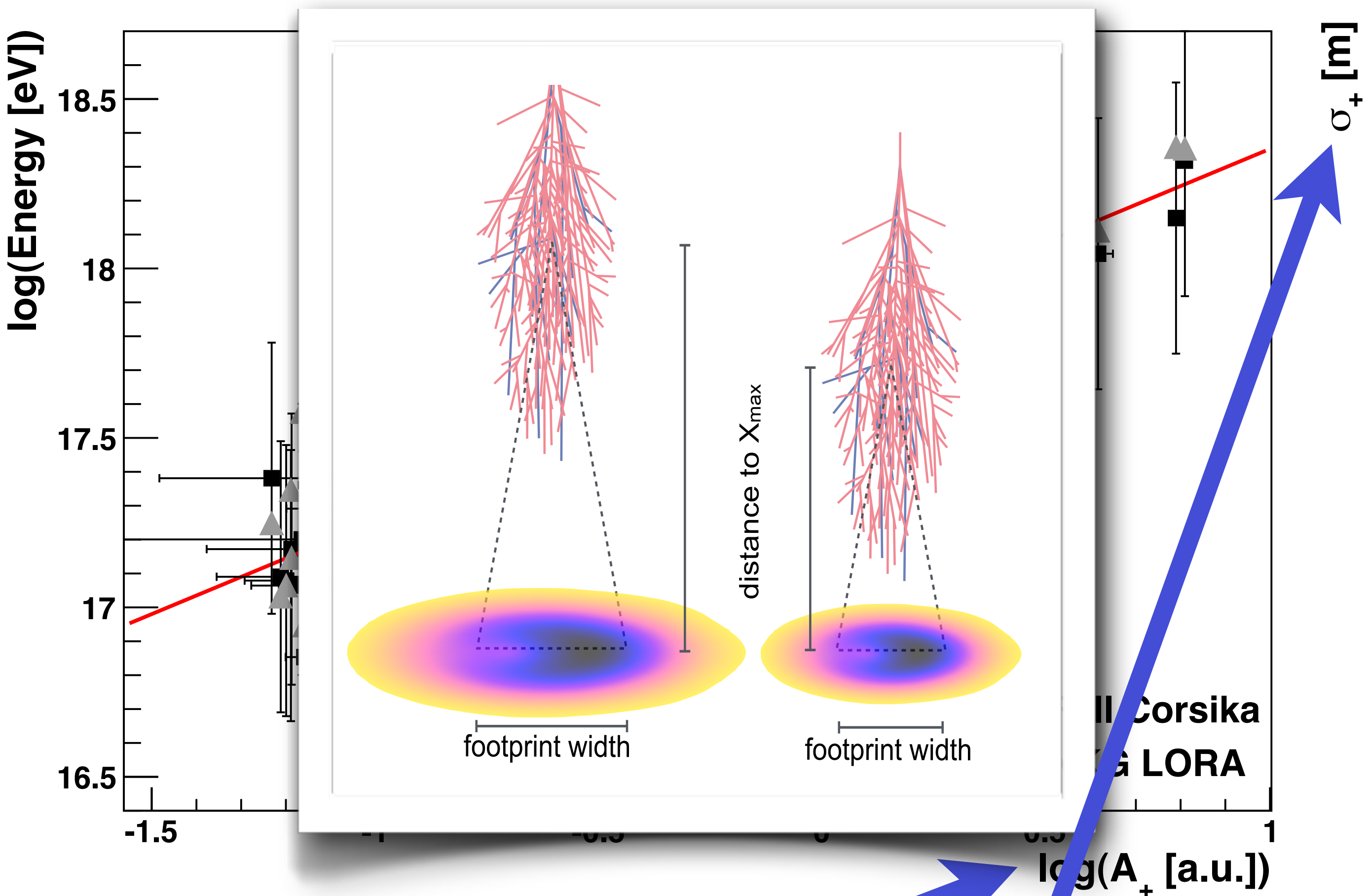

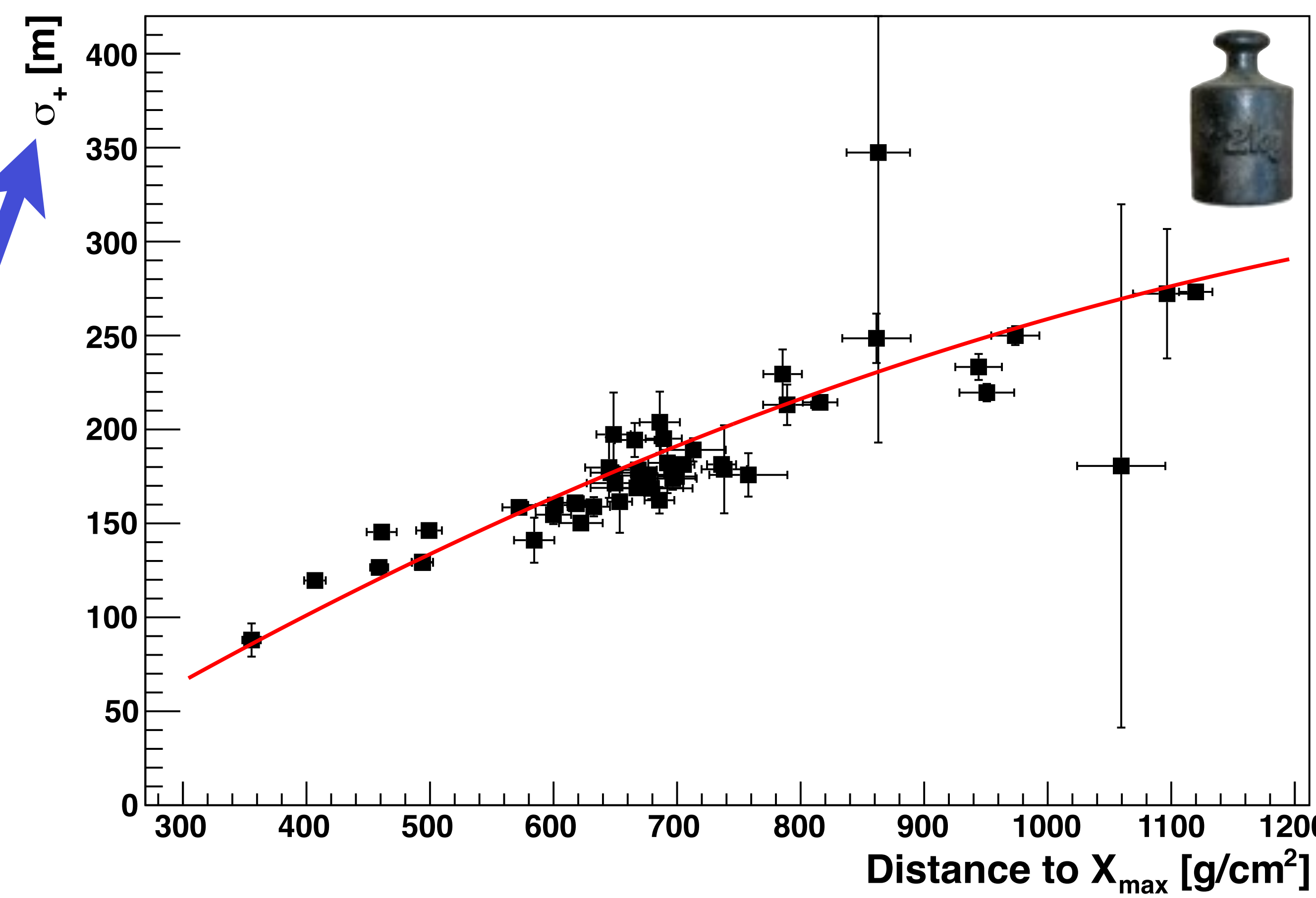

$$P(x',y') = A_{+} \cdot \exp\left(\frac{-[(x'-X_{+})^2 + (y'-Y_{+})^2]}{\sigma_{+}^2}\right) - A_{-} \cdot \exp\left(\frac{-[(x'-X_{-})^2 + (y'-Y_{-})^2]}{\sigma_{-}^2}\right) + O$$

LOFAR

A. Nelles et al., JCAP 05 (2015) 018

Measurement of particle mass

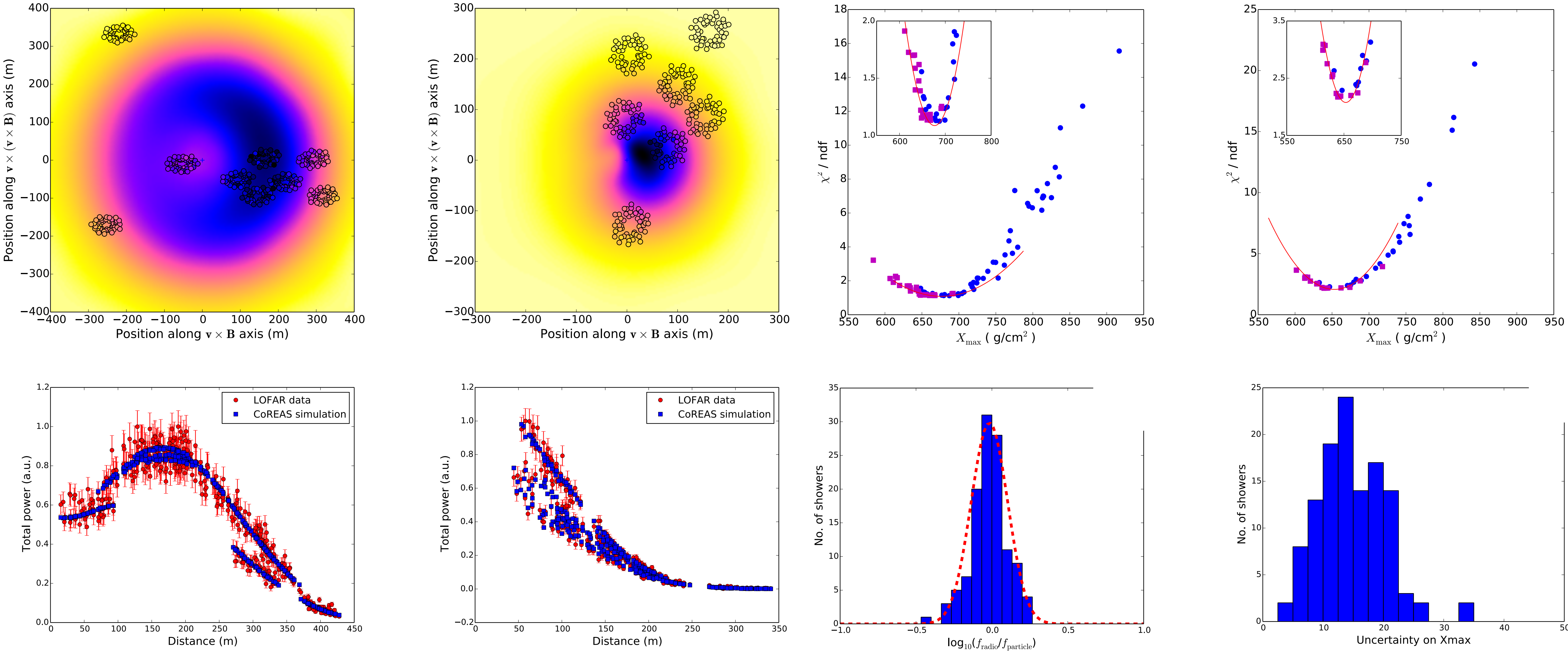

$$\sigma_E \approx 32\%$$

$$\sigma_{X_{max}} \approx 17\ \mathrm{g/cm^2}$$

S. Buitink et al., PRD 90 (2014) 082003

Depth of the shower maximum

LETTER nature

doi:10.1038/nature16976

A large light-mass component of cosmic rays at 10^{17}–$10^{17.5}$ electronvolts from radio observations

S. Buitink[1,2], A. Corstanje[2], H. Falcke[2,3,4,5], J. R. Hörandel[2,4], T. Huege[6], A. Nelles[2,7], J. P. Rachen[2], L. Rossetto[2], P. Schellart[2], O. Scholten[8,9], S. ter Veen[3], S. Thoudam[2], T. N. G. Trinh[8], J. Anderson[10], A. Asgekar[3,11], I. M. Avruch[12,13], M. E. Bell[14], M. J. Bentum[3,15], G. Bernardi[16,17], P. Best[18], A. Bonafede[19], F. Breitling[20], J. W. Broderick[21], W. N. Brouw[3,13], M. Brüggen[19], H. R. Butcher[22], D. Carbone[23], B. Ciardi[24], J. E. Conway[25], F. de Gasperin[19], E. de Geus[3,26], A. Deller[3], R.-J. Dettmar[27], G. van Diepen[3], S. Duscha[3], J. Eislöffel[28], D. Engels[29], J. E. Enriquez[3], R. A. Fallows[3], R. Fender[30], C. Ferrari[31], W. Frieswijk[3], M. A. Garrett[3,32], J. M. Grießmeier[33,34], A. W. Gunst[3], M. P. van Haarlem[3], T. E. Hassall[21], G. Heald[3,13], J. W. T. Hessels[3,23], M. Hoeft[28], A. Horneffer[5], M. Iacobelli[3], H. Intema[32,35], E. Juette[27], A. Karastergiou[30], V. I. Kondratiev[3,36], M. Kramer[5,37], M. Kuniyoshi[38], G. Kuper[3], J. van Leeuwen[3,23], G. M. Loose[3], P. Maat[3], G. Mann[20], S. Markoff[23], R. McFadden[3], D. McKay-Bukowski[39,40], J. P. McKean[3,13], M. Mevius[3,13], D. D. Mulcahy[21], H. Munk[3], M. J. Norden[3], E. Orru[3], H. Paas[41], M. Pandey-Pommier[42], V. N. Pandey[3], M. Pietka[30], R. Pizzo[3], A. G. Polatidis[3], W. Reich[5], H. J. A. Röttgering[32], A. M. M. Scaife[21], D. J. Schwarz[43], M. Serylak[30], J. Sluman[3], O. Smirnov[17,44], B. W. Stappers[37], M. Steinmetz[20], A. Stewart[30], J. Swinbank[23,45], M. Tagger[33], Y. Tang[3], C. Tasse[44,46], M. C. Toribio[3,32], R. Vermeulen[3], C. Vocks[20], C. Vogt[3], R. J. van Weeren[16], R. A. M. J. Wijers[23], S. J. Wijnholds[3], M. W. Wise[3,23], O. Wucknitz[5], S. Yatawatta[3], P. Zarka[47] & J. A. Zensus[5]

Cosmic rays are the highest-energy particles found in nature. Measurements of the mass composition of cosmic rays with energies of 10^{17}–10^{18} electronvolts are essential to understanding whether they have galactic or extragalactic sources. It has also been proposed that the astrophysical neutrino signal[1] comes from accelerators capable of producing cosmic rays of these energies[2]. Cosmic rays initiate air showers—cascades of secondary particles in the atmosphere—and their masses can be inferred from measurements of the atmospheric depth of the shower maximum[3] (X_{max}; the depth of the air shower when it contains the most particles) or of the composition of shower particles reaching the ground[4]. Current measurements[5] have either high uncertainty, or a low duty cycle and a high energy threshold. Radio detection of cosmic rays[6–8] is a rapidly developing technique[9] for determining X_{max} (refs 10, 11) with a duty cycle of, in principle, nearly 100 per cent. The radiation is generated by the separation of relativistic electrons and positrons in the geomagnetic field and a negative charge excess in the shower front[6,12]. Here we report radio measurements of X_{max} with a mean uncertainty of 16 grams per square centimetre for air showers initiated by cosmic rays with energies of 10^{17}–$10^{17.5}$ electronvolts. This high resolution in X_{max} enables us to determine the mass spectrum of the cosmic rays: we find a mixed composition, with a light-mass fraction (protons and helium nuclei) of about 80 per cent. Unless, contrary to current expectations, the extragalactic component of cosmic rays contributes substantially to the total flux below $10^{17.5}$ electronvolts, our measurements indicate the existence of an additional galactic component, to account for the light composition that we measured in the 10^{17}–$10^{17.5}$ electronvolt range.

Observations were made with the Low Frequency Array (LOFAR[13]), a radio telescope consisting of thousands of crossed dipoles with built-in air-shower-detection capability[14]. LOFAR continuously records the radio signals from air showers, while simultaneously running astronomical observations. It comprises a scintillator array (LORA) that triggers the read-out of buffers, storing the full waveforms received by all antennas.

We selected air showers from the period June 2011 to January 2015 with radio pulses detected in at least 192 antennas. The total uptime was about 150 days, limited by construction and commissioning of the

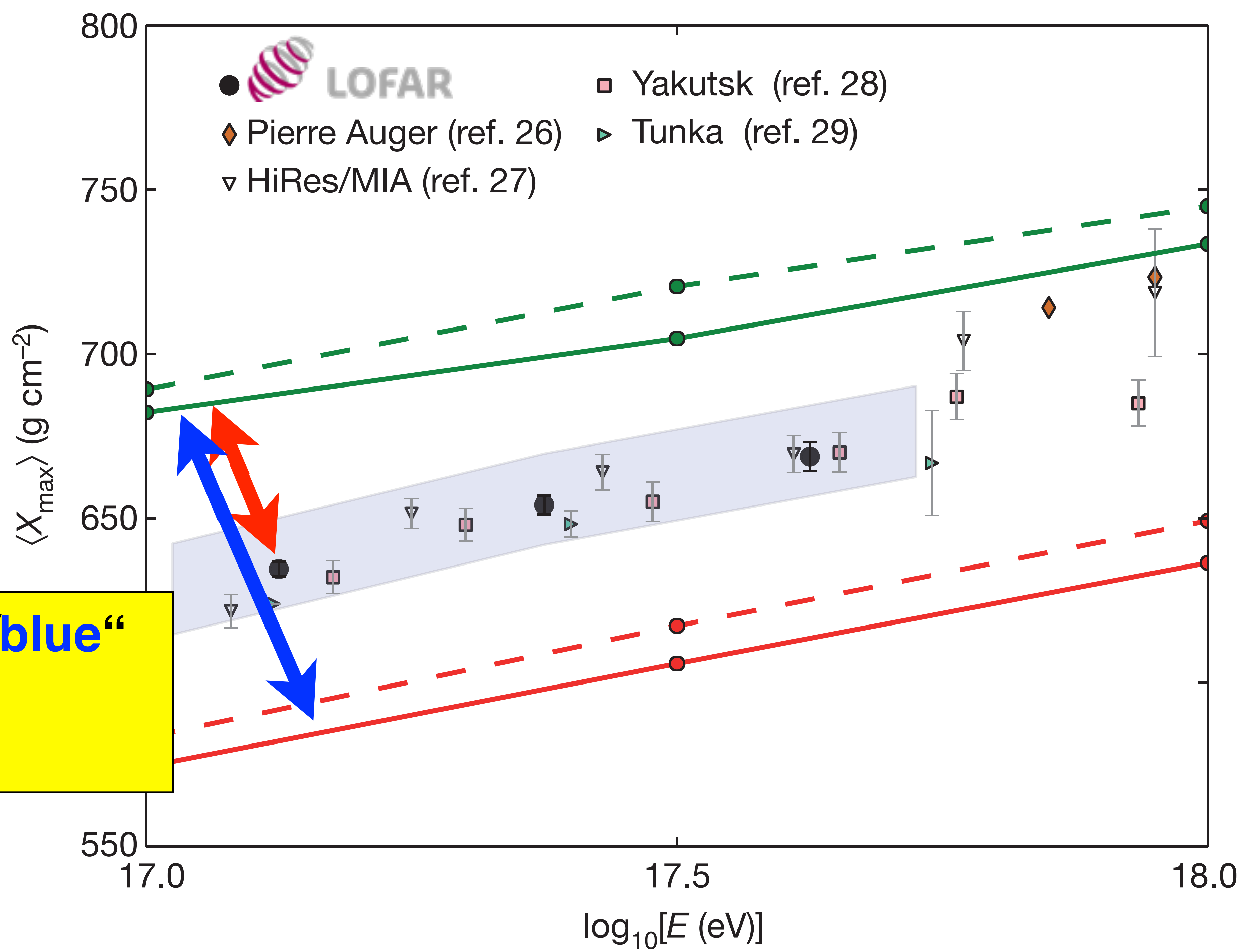

relative distance "red/blue" is measure for ln A (particle type)

S. Buitink et al., Nature 531 (2016) 70

Mean logarithmic mass

$$\ln A = \sum k_i \ln A_i$$

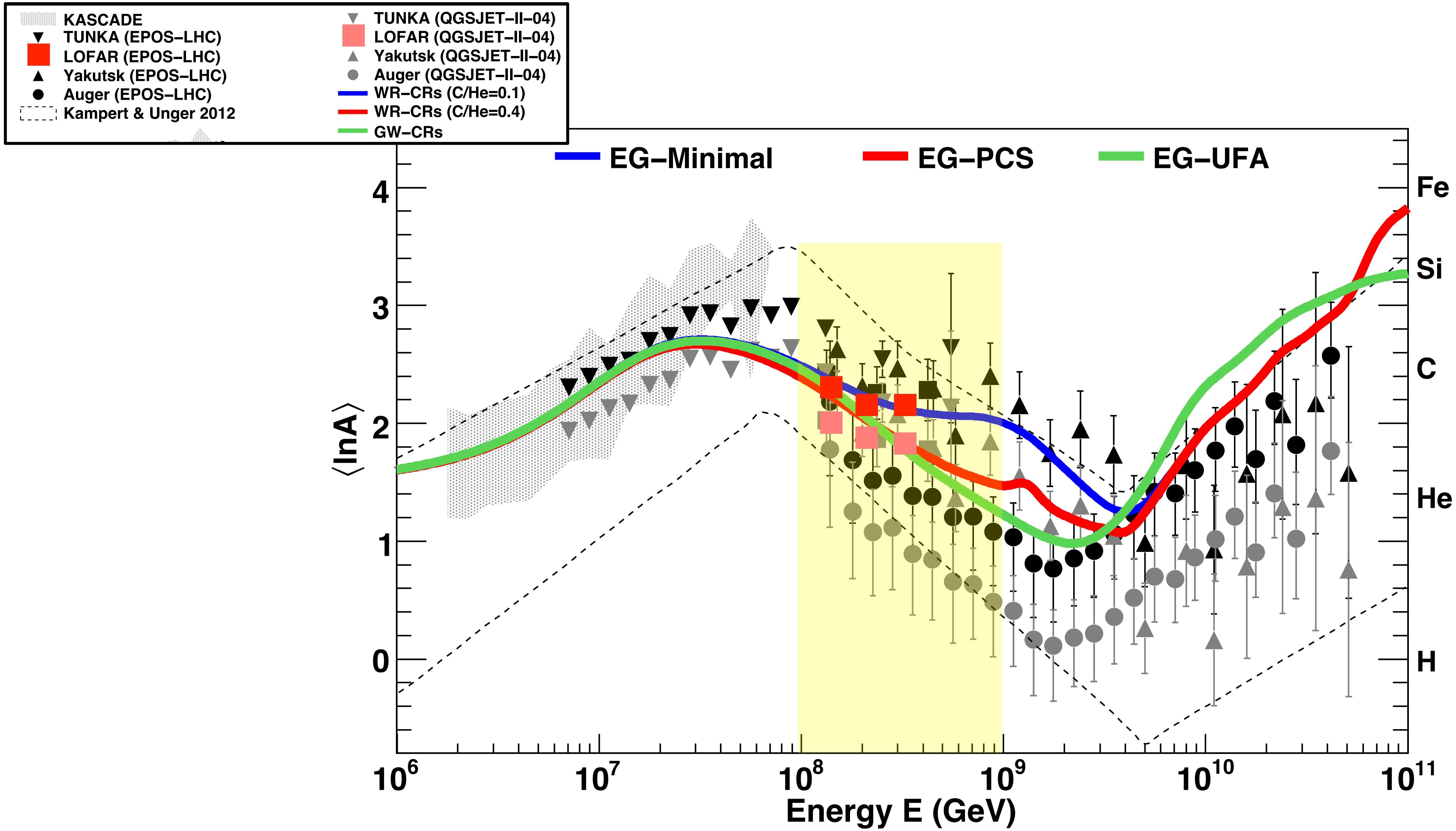

S. Thoudam et al., A&A in press (2016), arXiv 1605.03111

A&A 567, A33 (2014)
DOI: 10.1051/0004-6361/201322996

Astronomy & Astrophysics

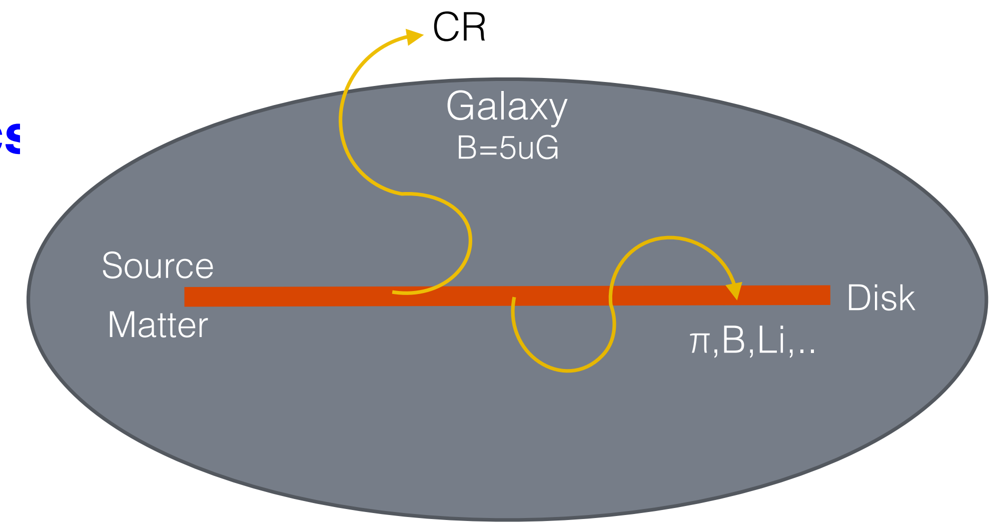

GeV-TeV cosmic-ray spectral anomaly as due to reacceleration by weak shocks in the Galaxy★

Satyendra Thoudam and Jörg R. Hörandel

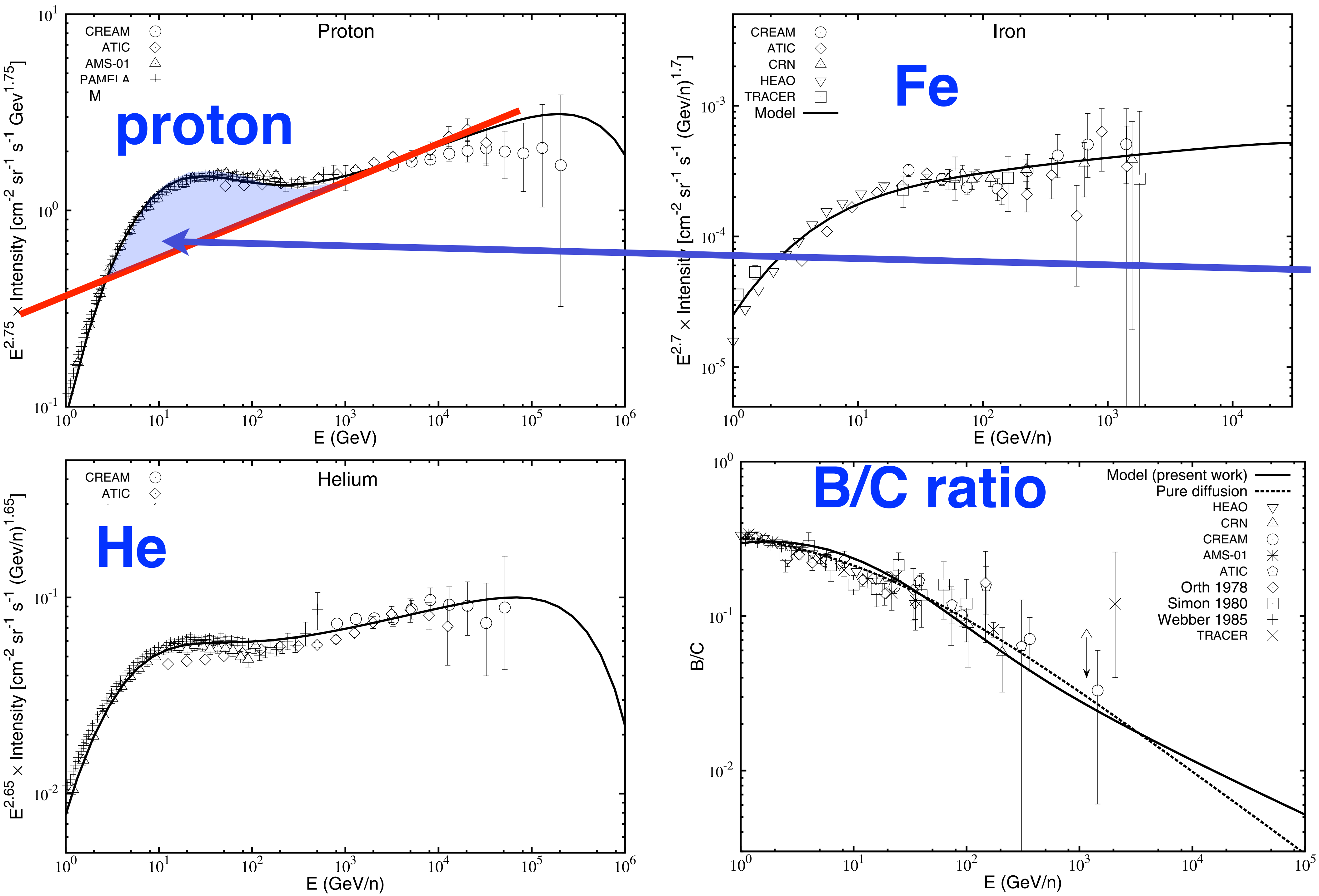

bump due to reacceleration by weak shocks in the Galaxy

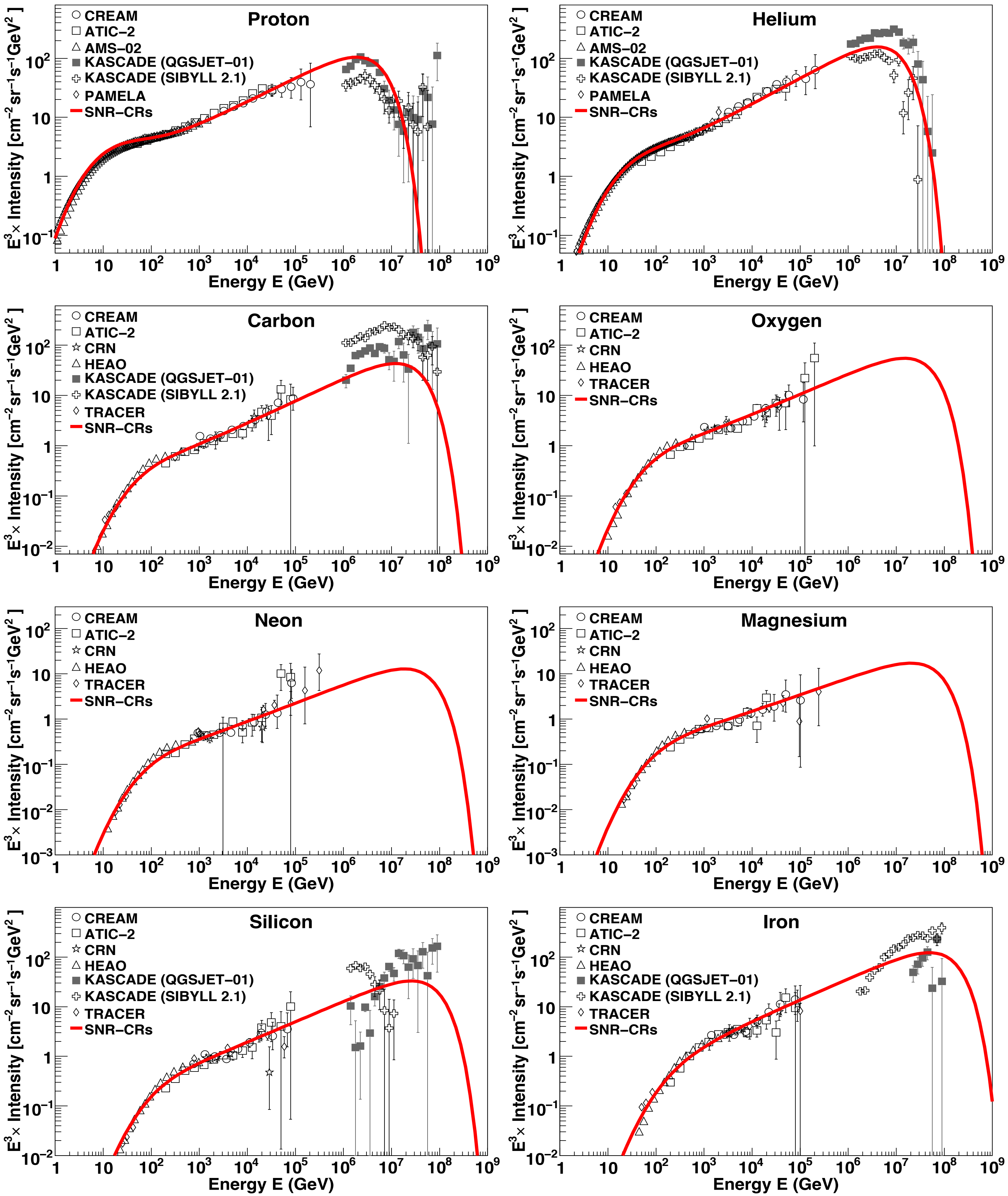

Fig. 1. Energy spectra for different cosmic-ray elements. *Solid line*: Model prediction for the SNR-CRs. *Data*: CREAM (Ahn et al. 2009; Yoon et al. 2011), ATIC-2 (Panov et al. 2007), AMS-02 (Aguilar et al. 2015a,b), PAMELA (Adriani et al. 2011), CRN (Müller et al. 1991; Swordy et al. 1990), HEAO (Engelmann et al. 1990), TRACER (Obermeier et al. 2011), and KASCADE (Antoni et al. 2005). Cosmic-ray source parameters (q, f) used in the calculation are given in Table 1. For the other model parameters (D_0, a, η, s), see text for details.

Contribution of (regular) SNR-CR

$$E_c = Z \cdot 4.5\ 10^6\ \mathrm{GeV}$$

$$Q(p) = AQ_0(Ap)^{-q} \exp\left(-\frac{Ap}{Zp_c}\right),$$

Table 1. Source spectral indices, q, and energy injected per supernova, f, for the different species of cosmic rays used in the calculation of the SNR-CRs spectra shown in Figures 1 and 2.

Particle type	q	f $(\times 10^{49}$ ergs)
Proton	2.24	6.95
Helium	2.21	0.79
Carbon	2.21	2.42×10^{-2}
Oxygen	2.25	2.52×10^{-2}
Neon	2.25	3.78×10^{-3}
Magnesium	2.29	5.17×10^{-3}
Silicon	2.25	5.01×10^{-3}
Iron	2.25	4.95×10^{-3}

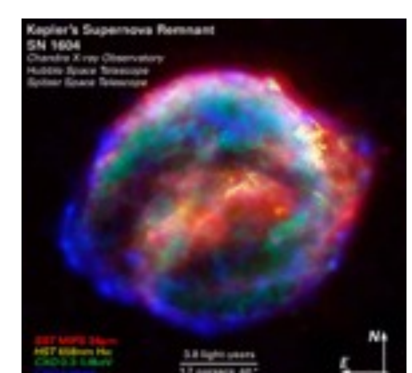

S. Thoudam et al., A&A in press (2016), arXiv 1605.03111

Contribution of (regular) SNR-CR to all-particle spectrum

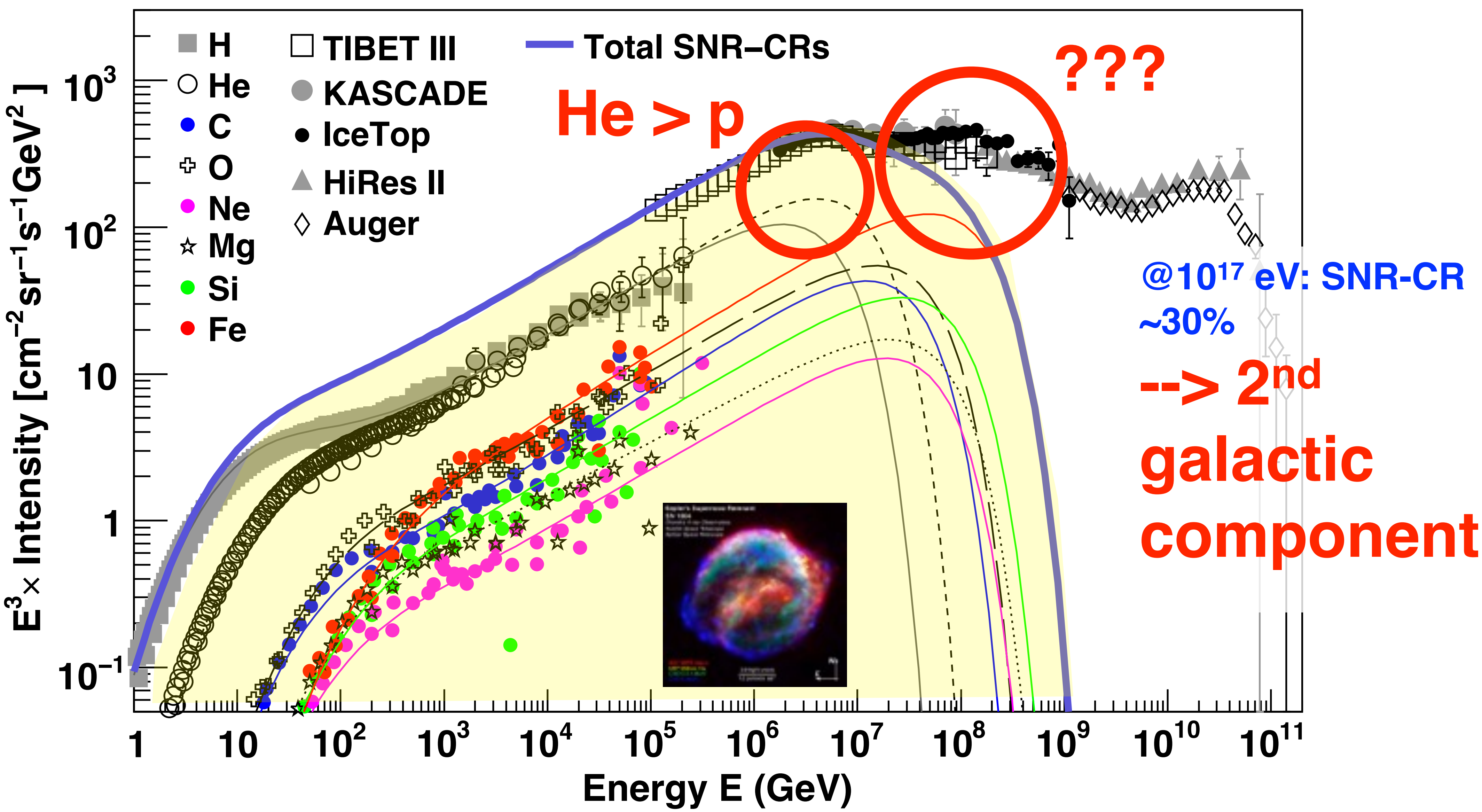

Fig. 2. Contribution of SNR-CRs to the all-particle cosmic-ray spectrum. The thin lines represent spectra for the individual elements, and the thick-solid line represents the total contribution. The calculation assumes an exponential cut-off energy for protons at $E_c = 4.5 \times 10^6$ GeV. Other model parameters, and the low-energy data are the same as in Figure 1. Error bars are shown only for the proton and helium data. High-energy data: KASCADE (Antoni et al. 2005), IceTop (Aartsen et al. 2013), Tibet III (Amenomori et al. 2008), the Pierre Auger Observatory (Schulz et al. 2013), and HiRes II (Abbasi et al. 2009).

~8% of mechanical power of SN --> CRs

S. Thoudam et al., A&A in press (2016), arXiv 1605.03111

Re-acceleration of SNR-CRs by Galactic wind termination shocks (GW-CRs)

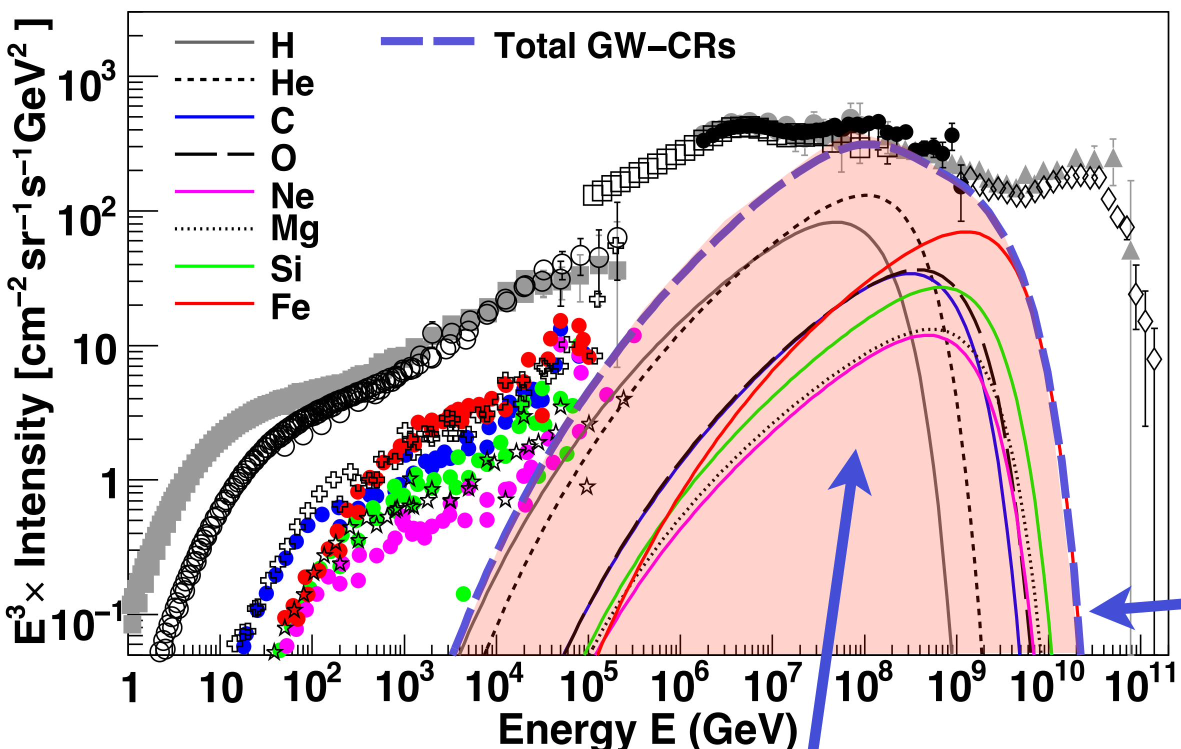

Fig. 3. Contribution of GW-CRs to the all-particle cosmic-ray spectrum. The thin lines represent spectra for the individual elements, and the thick dashed line represents the total contribution. The injection fraction, $k_w = 14.5\%$, and the exponential cut-off energy for protons, $E_{sh} = 9.5 \times 10^7$ GeV. See text for the other model parameters. Data are the same as in Figure 2.

fall-off due to exp fall-off in source spectra

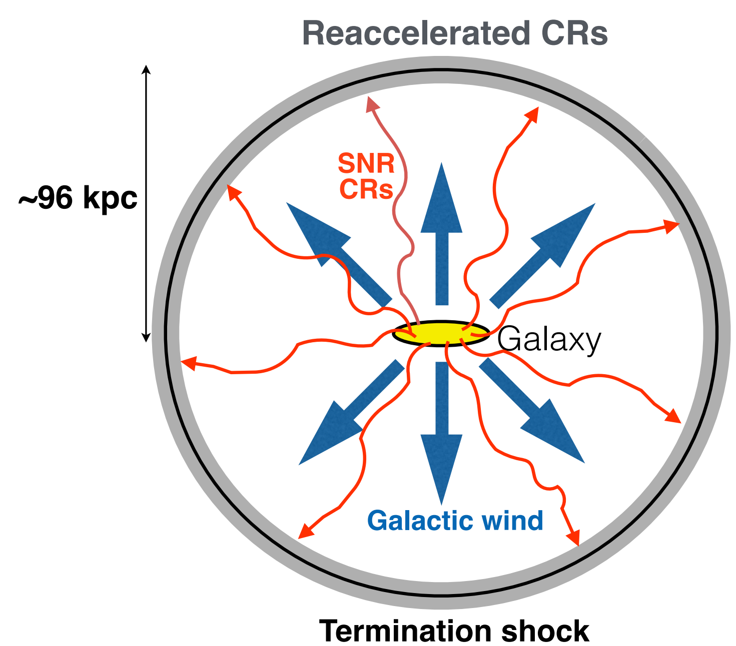

$$k_{sh} = 14.5\% \quad E_{sh} = 9.5 \cdot 10^7 \text{ GeV}$$

$$V = \dot{V} r \quad \dot{V} = 15 \text{ km/s/kpc}$$

S. Thoudam et al., A&A submitted (2016), arXiv 1605.03111

Cosmic rays from Wolf-Rayet star explosions (WR-CRs)

1/210 yr = 1/7 SN

Table 2. Relative abundances of different cosmic-ray species with respect to helium for two different Wolf-Rayet wind compositions used in our model (Pollock et al. 2005).

Particle type	C/He = 0.1	C/He = 0.4
Proton	0	0
Helium	1.0	1.0
Carbon	0.1	0.4
Oxygen	3.19×10^{-2}	7.18×10^{-2}
Neon	0.42×10^{-2}	1.03×10^{-2}
Magnesium	2.63×10^{-4}	6.54×10^{-4}
Silicon	2.34×10^{-4}	5.85×10^{-4}
Iron	0.68×10^{-4}	1.69×10^{-4}

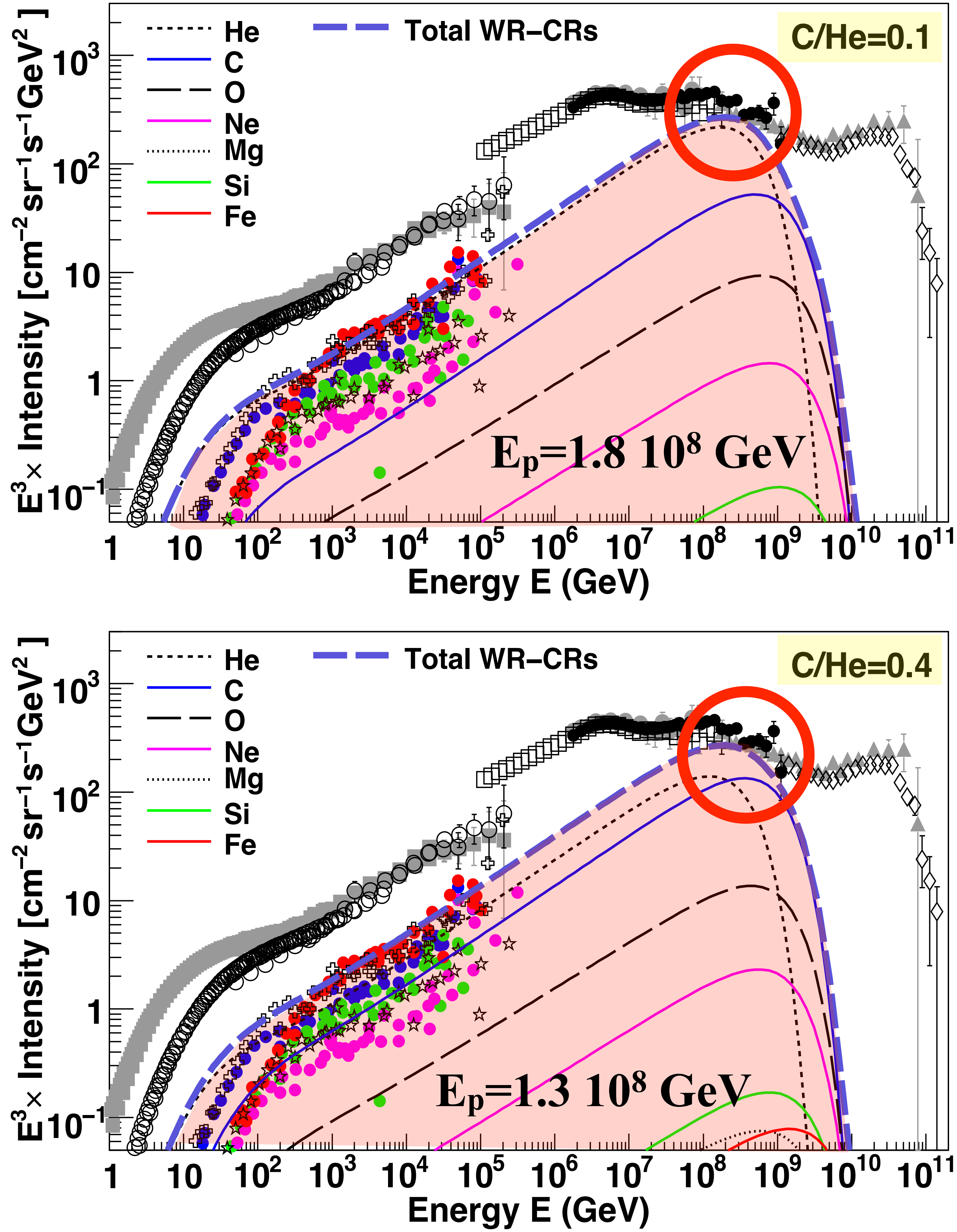

Fig. 4. Contribution of WR-CRs to the all-particle spectrum. *Top*: C/He = 0.1. *Bottom*: C/He = 0.4. The thin lines represent spectra for the individual elements, and the thick dashed line represents the total contribution. The calculation assumes an exponential energy cut-off for protons at $E_c = 1.8 \times 10^8$ GeV for C/He = 0.1, and $E_c = 1.3 \times 10^8$ GeV for C/He = 0.4. See text for the other model parameters. Data: same as in Figure 2.

S. Thoudam et al., A&A in press (2016), arXiv 1605.03111

all-particle spectra including 2nd galactic component

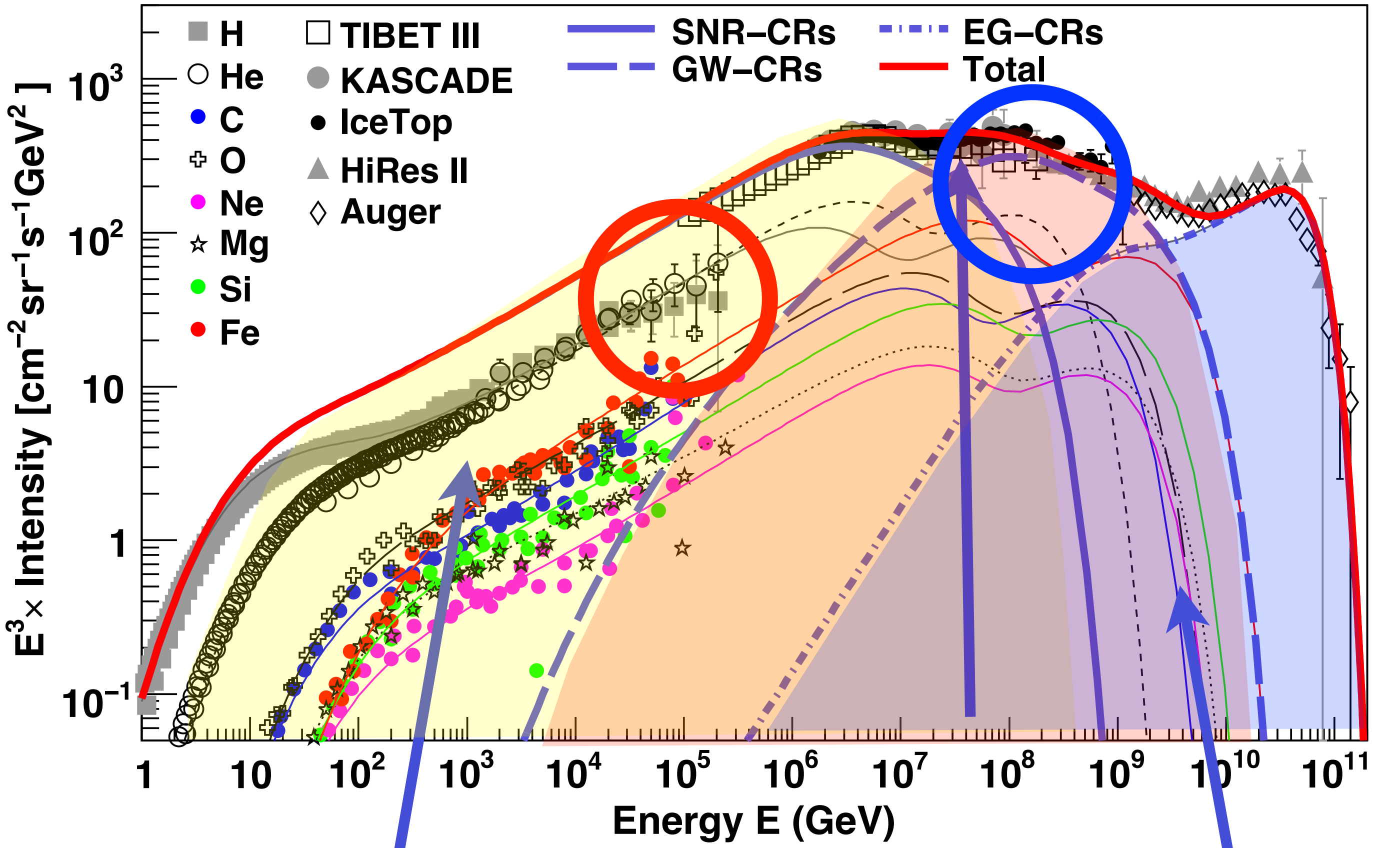

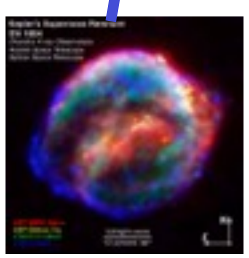

Table 3. Injection energy of SNR-CRs used in the calculation of all-particle spectrum in the WR-CR model (Figure 6).

Particle type	C/He = 0.1 $f(\times 10^{49}$ ergs)	C/He = 0.4 $f(\times 10^{49}$ ergs)
Proton	8.11	8.11
Helium	0.67	0.78
Carbon	2.11×10^{-2}	0.73×10^{-2}
Oxygen	2.94×10^{-2}	2.94×10^{-2}
Neon	4.41×10^{-3}	4.41×10^{-3}
Magnesium	6.03×10^{-3}	6.03×10^{-3}
Silicon	5.84×10^{-3}	5.84×10^{-3}
Iron	5.77×10^{-3}	5.77×10^{-3}

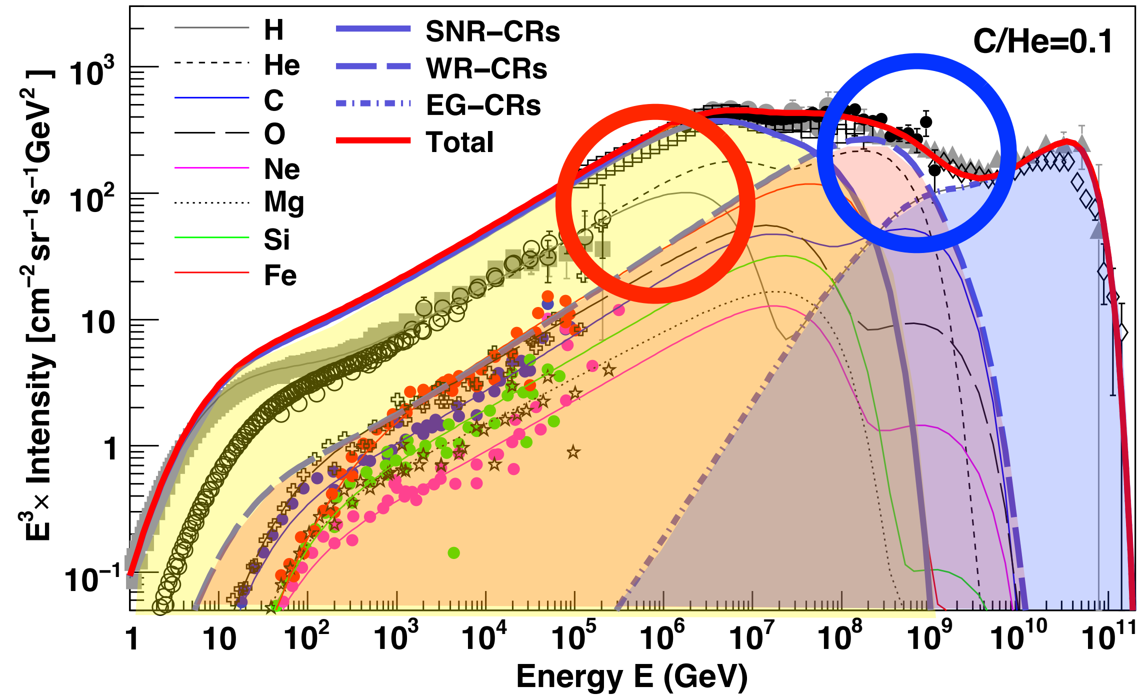

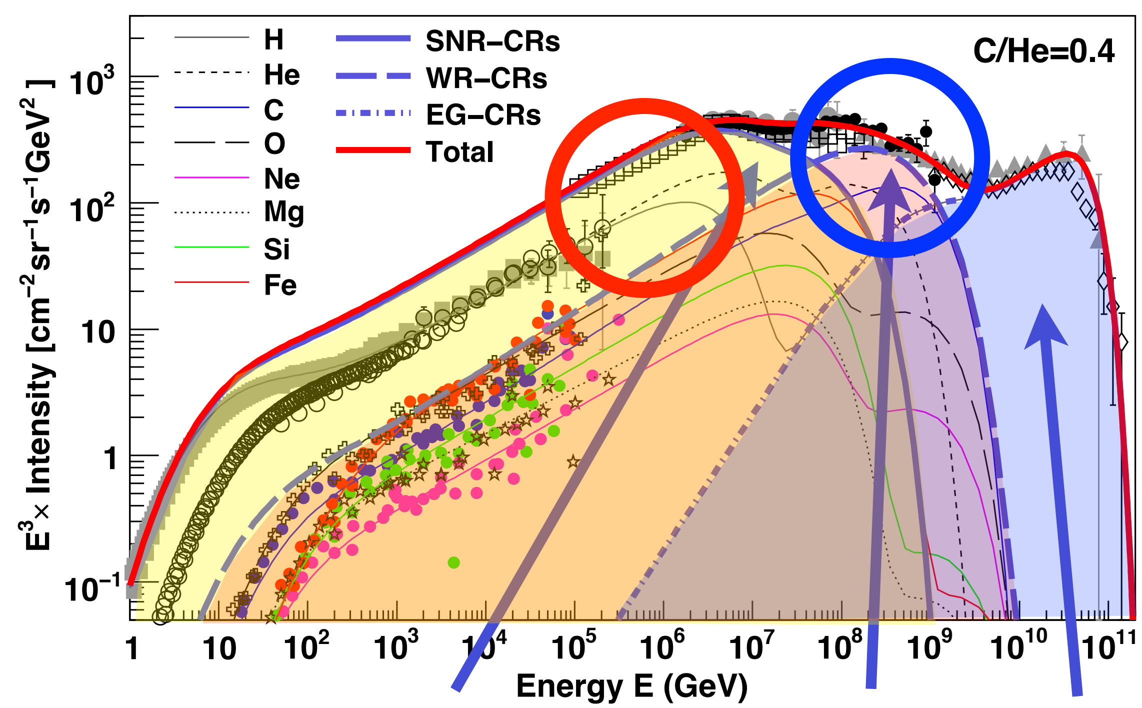

S. Thoudam et al., A&A submitted (2016), arXiv 1605.03111

All-particle energy spectrum - 3 components

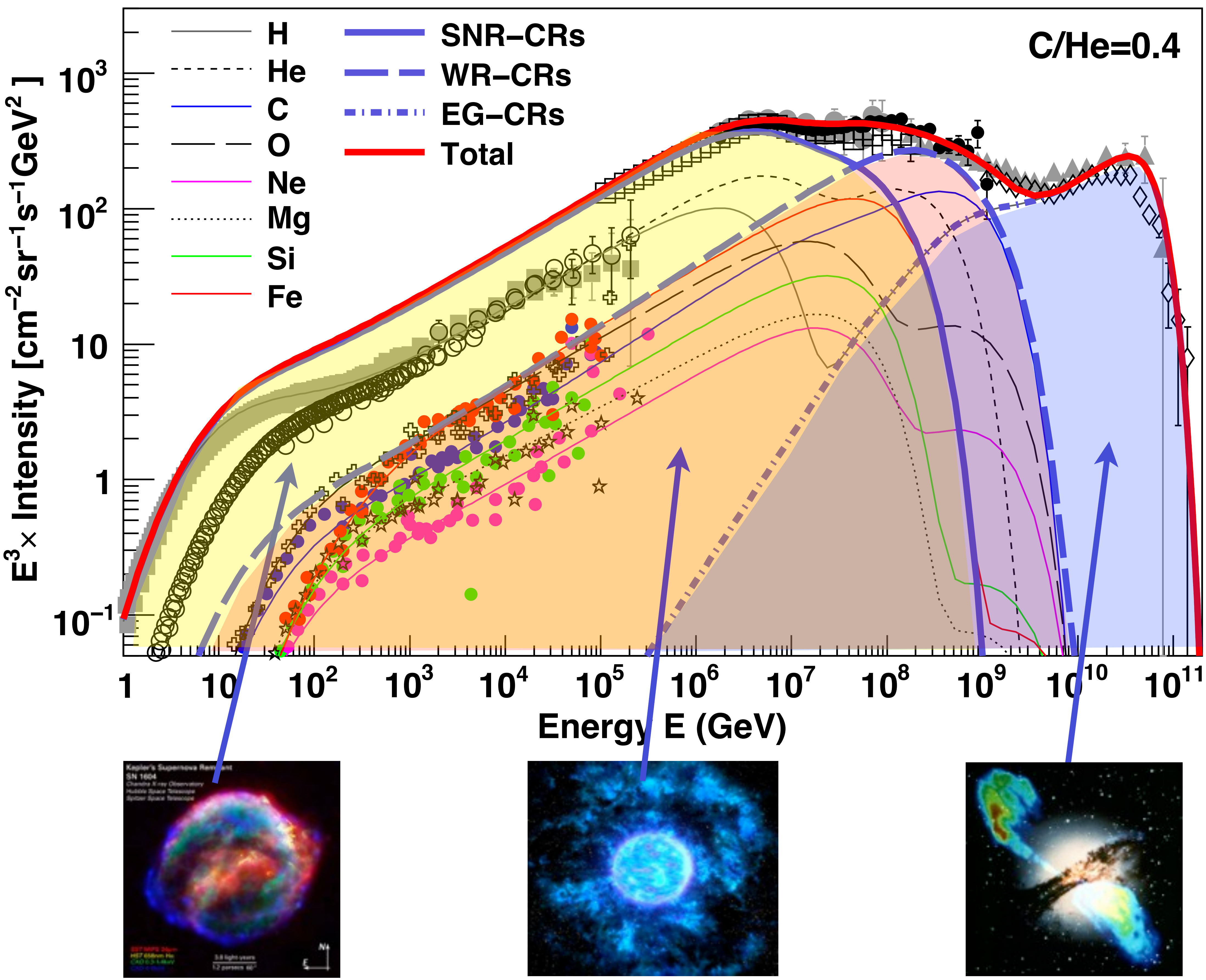

S. Thoudam et al., A&A in press (2016), arXiv 1605.03111